Molecular Dynamics Simulation of Grain Boundary Migration

Jian Zhou
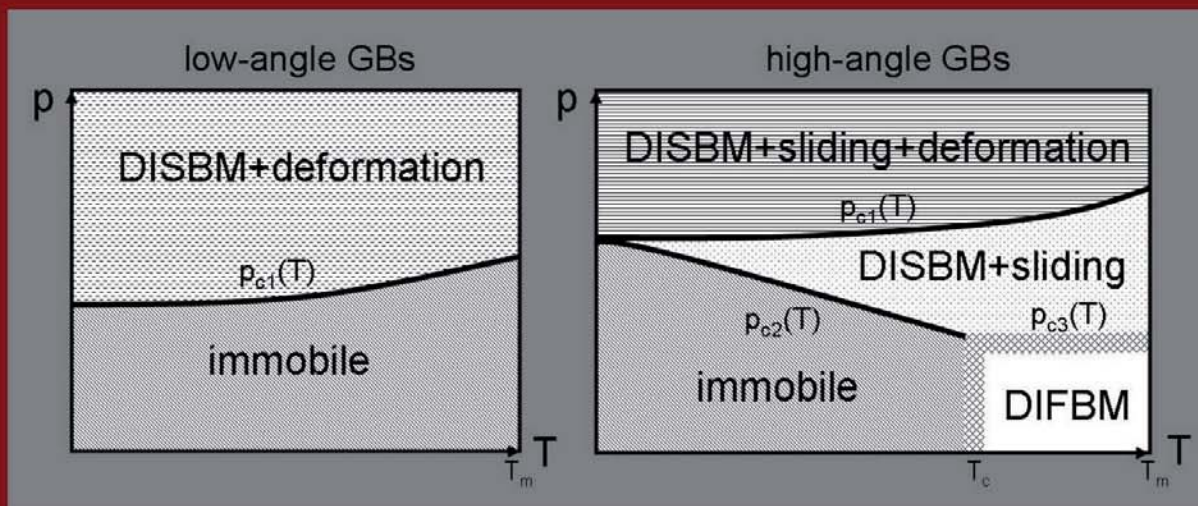
Molecular dynamics simulation of grain boundary migration

Molecular dynamics simulation of grain boundary migration

From the Faculty of Georesources and Materials Engineering of the
RWTH Aachen University

Submitted by

Jian Zhou, M.Sc.

from (Wujiang, China)

in respect of the academic degree of

Doctor of Engineering

approved thesis

Advisors: Univ.-Prof. Dr.rer. nat. Dr. h.c. Günter Gottstein

          PD Dr.rer. nat. Volker Mohles

          Prof. Dr.rer. nat. Lasar S. Shvindlerman

Date of the oral examination: 15.02.2012

Acknowledgement

In the past four years, my stay and research work at the Institute of Physical Metallurgy and Metal Physics have led me to become a materials scientist. The German style of doctoral training gives me several qualities: independence, scientific rigour and especially the way of doing research, i.e. thinking of materials processes based on physics. All of these in turn greatly attract my interests and continuously encourage me to never stop pursuing the truth even when encountering various difficulties. Since my research during the time period is a tortuous road, I have to say that the publication of this thesis cannot be accomplished without the help from the following people.

I would like to thank my supervisors Prof. Günter Gottstein and PD Volker Mohles. The constructive advices given by Prof. Gottstein always inspired much thinking and profoundly influenced my research direction. Dr. Mohles spent a long time in revising the manuscript of the thesis. Our discussion concerning boundary migration by dislocation motions has improved the quality of the thesis to a large extent.

I am grateful to Prof. Molodov and Prof. Shvindlerman for their helpful suggestions. During discussion, their rich knowledge and abundant experience in the field of grain boundary migration deeply impress me. The answers from them are always satisfactory and significantly advance my work.

I would like to express my gratitude to Matthias Loeck and Sergej Laiko for technical supports in terms of computer maintenance, and to secretaries Miriam Wulfes, Sabine Lakrache and Hanne Linckens for their patient assistance, particularly given that I cannot speak German.

Sincere thanks go to my colleagues: Dr. Yaping Lü, Thiemo Brüggemann, Feng Jiao, Dr. Bingbing Zhao, Marco Witte, Felix Ulomek, Jia Song, Lei Hu, Sijia Mu, Dr. Luis Antonio Barrales Mora, Dr. Weiping Hu and Dr. Talal Al Samman. Thank you all for your

I

understanding and help. The time we spent together is unforgettable and definitely makes a deep imprint in my life.

Finally, I would like to thank my parents, Yanliang Zhou and Jianxin Wu. As your only child, our long-distance separation year after year brings pressure and troubles to a traditional Chinese family. It is your support that makes me able to follow my heart and achieve my ideal.

Contents

Abbreviations and symbols

Abbreviations

GB	: **G**rain **B**oundary
MD	: **M**olecular **D**ynamics
FCC	: **F**ace-**C**entered **C**ubic
HCP	: **H**exagonal **C**lose-**P**acked
CSL	: **C**oincidence **S**ite **L**attice
DSC	: **D**isplacement **S**hift **C**omplete
GBD	: **G**rain **B**oundary **D**islocation
SGBD	: **S**econdary **G**rain **B**oundary **D**islocation
TB-SMA	: **T**ight **B**inding method with **S**econd-**M**oment **A**pproximation
LJ	: **L**ennard-**J**ones

Variable meaning

v	: boundary migration velocity
m	: boundary migration mobility
p	: driving force
m^*	: reduced mobility
κ	: boundary curvature
S	: activation entropy in terms of grain boundary migration
H	: activation enthalpy in terms of grain boundary migration
m_0	: preexponential factor in terms of grain boundary migration
θ	: boundary misorientation angle
w	: grain boundary thickness
ω	: attempting frequency
Ω	: atomic volume at 0 K
V	: average volume involved in atomic jumps that collectively cause grain boundary migration

| a_0 | : lattice constant at 0 K |
| T_m | : melting point/temperature |

Physical constants and units of key properties

k_B	: Boltzmann constant = 1.38×10^{-23} J/K
a_0	: lattice constant at 0 K = 4.05 Å for Al described by the TB-SMA potential
eV	: 1 eV = 1.602×10^{-19} J
Unit of driving force	: 1 eV/atom = 9.65 GPa at 0 K for Al
Unit of mobility	: $m^4J^{-1}s^{-1}$
Unit of activation enthalpy	: eV/atom

VI

Chapter 1

Introduction

Grain boundary migration is an important process during recrystallization and grain growth. The rate of migration determines the kinetics of these phenomena, and therefore is responsible for the evolution of microstructures, which have been proved to be closely related to many material properties. Nevertheless, little is known about the atomistic mechanisms in terms of grain boundary migration. Owing to the complicated geometry of a grain boundary with five degrees of freedom, the existing experimental techniques, e.g. transmission electron microscopy, to date are still unable to trace the atomic movements during grain boundary migration, especially at relatively high temperatures. These techniques therefore cannot effectively reveal the underlying mechanisms. Although there is no direct evidence, grain boundary migration has been implied to be related to types of diffusion processes (grain boundary diffusion and bulk diffusion) based on the fact that the migration and diffusion processes frequently possess nearly the same magnitude of activation enthalpy. In order to accurately determine atomic motions, the simulation technique molecular dynamics, which possesses profound advantages of high spatial and temporal resolutions, has been utilized. Some mechanisms have been observed. But these mechanisms seem to contradict each other, or they can only be applied to certain cases. The common feature of these mechanisms

obtained from simulations however indicates that grain boundary motion is not relevant to any diffusion process.

Besides the mechanisms of motion, grain boundary mobility is of great concern for industrial process optimization and modelling. This quantity can be accurately determined in well-designed bicrystalline experiments. However the difficulty of preparing bicrystals for various materials significantly limits the types of grain boundaries for study, such that it is hard to systematically measure the grain boundary mobility. In the past 15 years, the mobility for pure metals has also been evaluated and predicted through molecular dynamics simulations. The computed mobilities however are always found to be much larger than the maximum experimental data obtained in ultra-high-purity metals by one or more orders of magnitude. This drastic divergence is usually attributed to the absence of impurities in simulations, which are inevitably present in real materials. The impurities are expected to segregate in grain boundaries and therefore retard grain boundary motion significantly.

In this work, we exploit molecular dynamics to simulate grain boundary motion. We focus on <111> tilt grain boundaries in pure Al, since the motion of these grain boundaries plays an important role in microstructural evolution during recrystallization and grain growth for conventional metals, and also because there are existing experimental data obtained in bicrystals for direct comparisons. The migration of the selected grain boundaries has been simulated in a wide temperature range with various magnitudes of driving force.

The contents of this work are organized as follows. In Chapter 2, the basics of grain boundary structure and its migration process are introduced on a general level. Together, the existing mechanisms regarding grain boundary migration and the mobility simulations performed previously by other groups are reviewed, respectively. Chapter 3 presents the simulation techniques relevant to this work. The techniques are mainly composed of molecular dynamics and the implementation of driving force for inducing grain boundary motion. In Chapter 4, the simulation results are provided. Based on these results as well as corresponding discussion, mechanism maps are proposed for boundary migration in polycrystals. In Chapter 5, we further concentrate on the boundary motion at a high temperature to compute mobilities, which are directly compared with experimental results. Finally, Chapter 6 gives a summary.

Chapter 2

Fundamentals

2.1 Grain boundary structure

A grain boundary (GB) is an internal interface which separates two grains of the same crystallography. On a macro level, there are in total eight geometric parameters required to comprehensively characterize a GB. As shown in Fig. 2.1, between the two adjacent grains, three parameters define a rotation angle θ of the crystal lattice (called misorientation in the context) about a common axis; the two parameters of the normalized boundary normal $\bar{n}$ describe the spatial orientation of the boundary plane; the last three parameters comprising a translation vector $\bar{t}$ denote the relative shift between identical lattice points in the two grains of the same material. In reality, when investigating the relation between a GB and its properties, the translation vector is usually neglected, possibly because the vector is hard to be measured experimentally and also its effect on dynamic processes might be trivial. However some simulations [1] to calculate the global minimum of grain boundary energy indeed indicate that the translation vector plays an important role. By altering the vector and then relaxing boundary structure sufficiently, it is found that there are a large number of local minima of GB energy together with substantial energetic barriers among them. The differences among the minima can be large [1]. For example, the energy difference is as large

as about 30% for a θ = 86.63° <110> tilt GB in a general face-centered cubic (FCC) metal. The specific number of the energy minima is found to be a function of GB type as well as temperature. The question whether the translation vector also has an effect on a dynamic process, e.g. GB migration, is unclear. To avoid much complexity, the vector is not taken into consideration in this work. Only the misorientation and the spatial orientation of boundary plane are focused on.
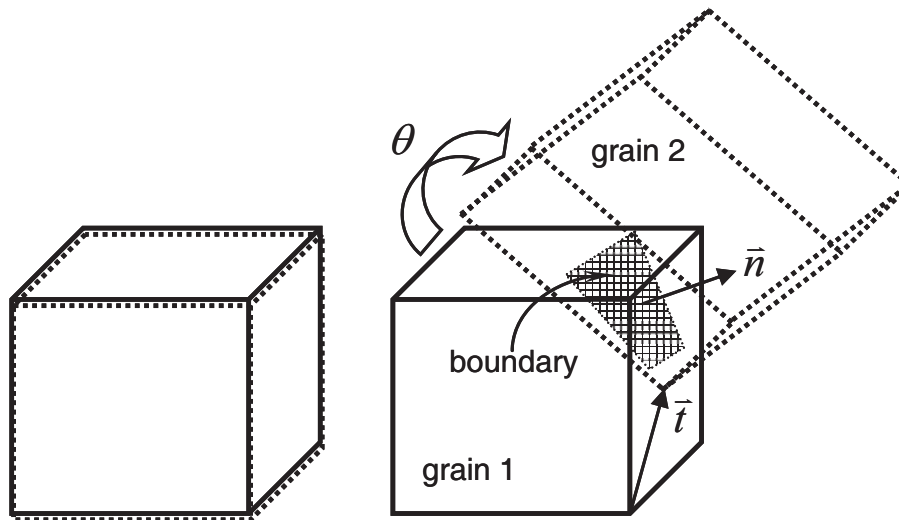
Fig. 2.1. Parameters for a geometrical description of a grain boundary.

Between the rotation axis and the boundary plane, there are distinct relations which give rise to different types of GBs. In the cases that the axis is perpendicular to the plane, twist GBs are obtained (Fig. 2.2a). When the axis is parallel to the plane, we have tilt GBs, which are further classified into symmetric or asymmetric ones, depending on whether the boundary normal has an identical or different description in the two adjoining grains, respectively (Fig. 2.2b). In comparison with the unique symmetric tilt GB for a given pair of a rotation axis and angle, an infinite number of asymmetric ones can occur.
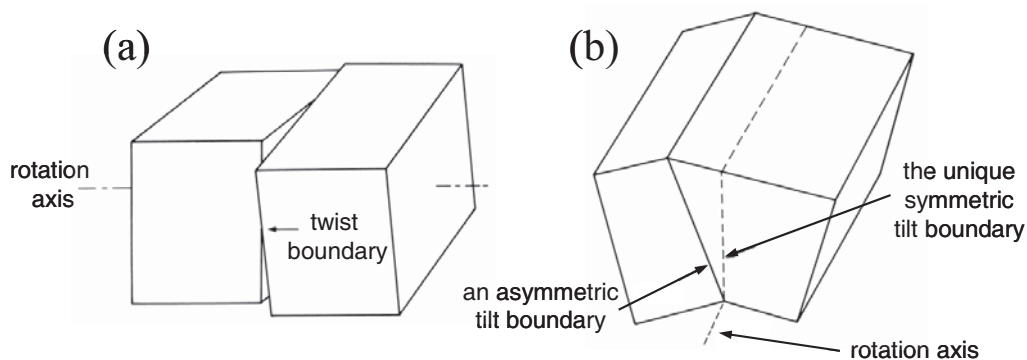
Fig. 2.2. Orientation of grain boundaries and rotation axes for different types of grain boundaries. (a) A twist boundary; (b) a symmetric and an asymmetric tilt boundary. (after[2])

From a microscopic view, GBs are composed of atoms in arrangements different from the one for a perfect crystal. The arrangement of boundary atoms reveals profound dissimilarity for GBs of small and large misorientations, i.e. so-called low-angle and high-angle GBs with a threshold θ of about 15°. Low-angle GBs are formed by dislocation arrays together with nearly-perfect crystal regions. For a symmetric low-angle tilt GB, as drawn schematically in Fig. 2.3, a set of edge dislocations regularly distribute along the boundary plane with a spacing d, which can be calculated by $d = b/\theta$ (b denotes the magnitude of Burgers vector associated with the edge dislocation), to create the misorientation. For an asymmetric tilt and a twist low-angle GBs, at least two sets of edge and screw dislocations, respectively, are needed. Since all these dislocations reside in GBs, they are named grain boundary dislocations (GBDs).
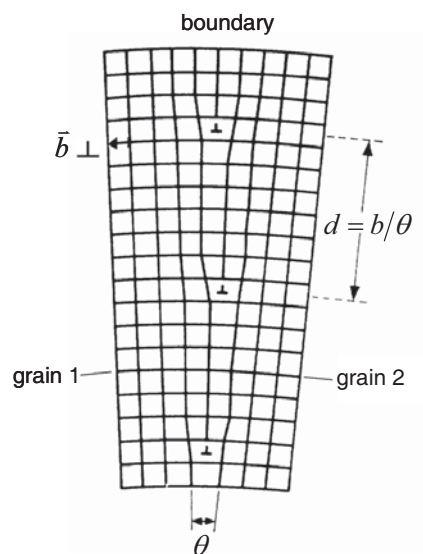
Fig. 2.3. Schematic of a low-angle tilt grain boundary formed by regularly distributed edge dislocations in nearly-perfect crystal regions. (after [2])

As indicated in Fig. 2.3, an increase in misorientation decreases the dislocation spacing, causing dislocation cores to come close to each other. When the misorientation becomes larger than about 15°, dislocation cores overlap substantially such that singular dislocations cannot be identified any more. The corresponding GBs are referred to as high-angle GBs. Although the structure of high-angle GBs might be thought of as a layer of disordered atoms, there are special misorientations which may provide GBs of relatively low energy. These misorientations refer to the cases when a coincidence site lattice (CSL) is generated. The 3-dimentional CSL represents an artificial lattice whose atomic positions are shared by the two adjacent crystals with the assumption that both crystal lattices are infinitely extended (Fig. 2.4). Since the two crystal lattices are periodic, the CSL must be periodic as well. Associated

with CSL, a quantity Σ, defined as the density ratio of ideal lattice sites to coincidence sites, then is commonly utilized to represent the corresponding misorientation and in turn the GB type. It should be noted that the CSL model merely concerns misorientation, but not a boundary plane. In practice, curved GBs frequently existing in polycrystals prevent unambiguous characterization of a specific boundary plane, thus misorientation is the unique measurable quantity. Using Σ to describe GBs of special misorientation becomes plausible. By contrast, for flat tilt GBs, misorientation together with a specific boundary plane need to be determined to comprehensively understand or describe a structure-property relation.
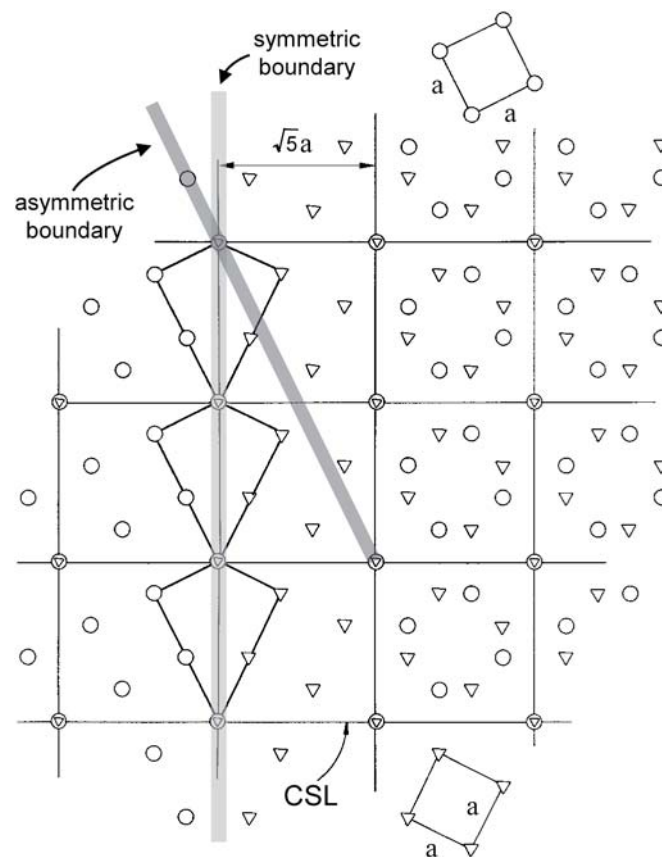
Fig. 2.4. Coincidence site lattice (CSL) and the structures of a twist GB (parallel to the paper plane shown on the right side), a symmetric tilt and an asymmetric tilt GB (both perpendicular to the paper plane given on the left side) in a cubic crystal lattice. All three GBs possess the same misorientation of 36.87° around the <100> axis in a cubic crystal. These GBs are also of the same Σ equal to 5. The circles and triangles represent atoms in two grains, respectively. The lattice constant is denoted by a.
(after [2])

As implied in the CSL constructuion, the Σ misorientations are discrete. When there is a deviation from these misorientations, it is proposed that a network of grain boundary dislocations is generated in GBs. These dislocations are of Burgers vectors of the displacement shift complete (DSC) lattice, which is the coarsest grid that comprises all lattice points of both crystal lattices (Fig. 2.5). Since the magnitudes of the Burgers vectors

associated with these GB dislocations are smaller than the ones for lattice dislocations, these dislocations are called secondary GB dislocations (SGBDs). The introduction of SGBD into Σ misorientation nevertheless still cannot compensate the deviation thoroughly, since the DSC lattice is discrete as well. For continuously changing misorientation, there must be cases for which other types of defects, e.g. local lattice distortion, take place.
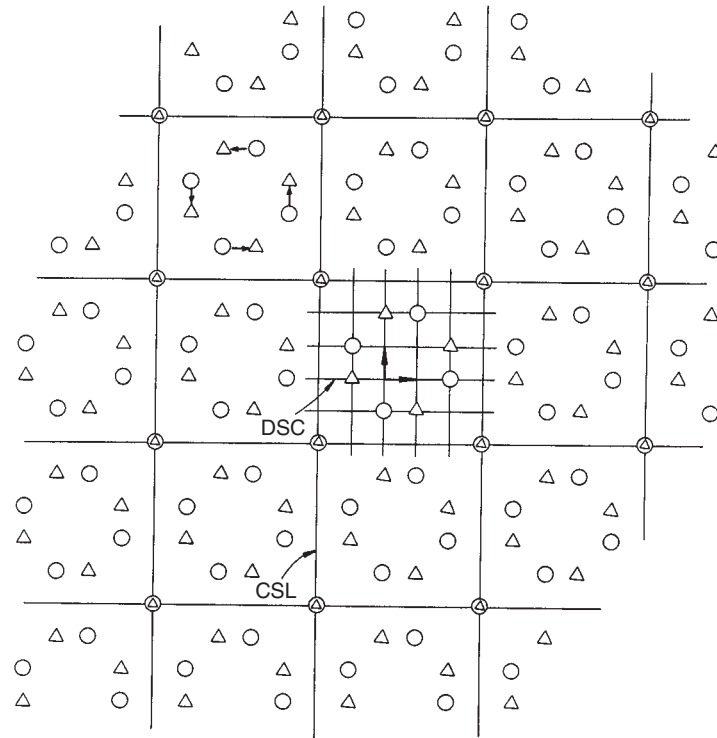
Fig. 2.5. Coincidence site lattice (CSL) and displacement shift complete (DSC) lattice for a 36.87° <100> twist grain boundary in cubic crystals. (after [2])

It should be noted that the question how special the Σ GBs are is subtle. Considering the relation between properties and misorientation, only very few GBs with low Σ values may reveal low boundary energy, while the others exhibit uniform high energy almost identical to the magnitude associated with GBs of general misorientations (Fig. 2.6). A correlation between kinetic parameters (GB migration mobility and its activation parameters) and the Σ misorientations is found in some studies, but not in others. In this sense, Wolf et al. [3] suggested that high-angle GBs should be classified into two types: special and general GBs. The former only concerns the Σ GBs giving rise to energy cusps (Fig. 2.6). All the other GBs pertain to general GBs. This suggestion is adopted in this work.
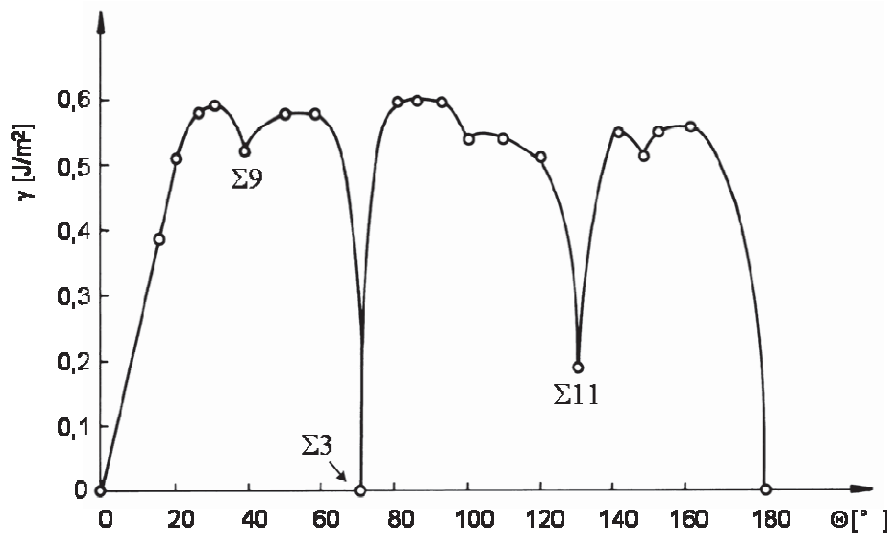
Fig. 2.6. Misorientation dependence of grain boundary energy for symmetric <110> tilt boundaries in Al. The energy cusps are associated with several low-Σ GBs. (after [4])

Up to now, the consideration of high-angle GB structure is confined to purely geometrical descriptions. According to Fig. 2.4, one may notice that there are large spaces present in the symmetric tilt GB. This structure is expected to be of high energy and thus being unstable. To lower the boundary energy, a structural relaxation takes place. The relaxation process usually doesn't change the periodicity of the CSL. But short-range shifts of atomic positions cause GBs to exhibit some structural disorder. Based on the analyses in terms of GB atoms through the radial distribution function, the structure of a high-angle GB at low temperatures is demonstrated to be solid-like, resembling glass [3, 5], as shown in Fig. 2.7a. The degree of the disorder is limited, as GBs still can be described by some kite-shaped structural units (Fig. 2.8). With increasing temperature, the disorder becomes further enhanced. For a temperature higher than a critical point, a high-angle GB undergoes a reversible structural transformation to be liquid-like in analogy to a bulk melt [3, 5], as illustrated in Fig. 2.7b. This transformation process is also referred to as GB premelting [6-9].
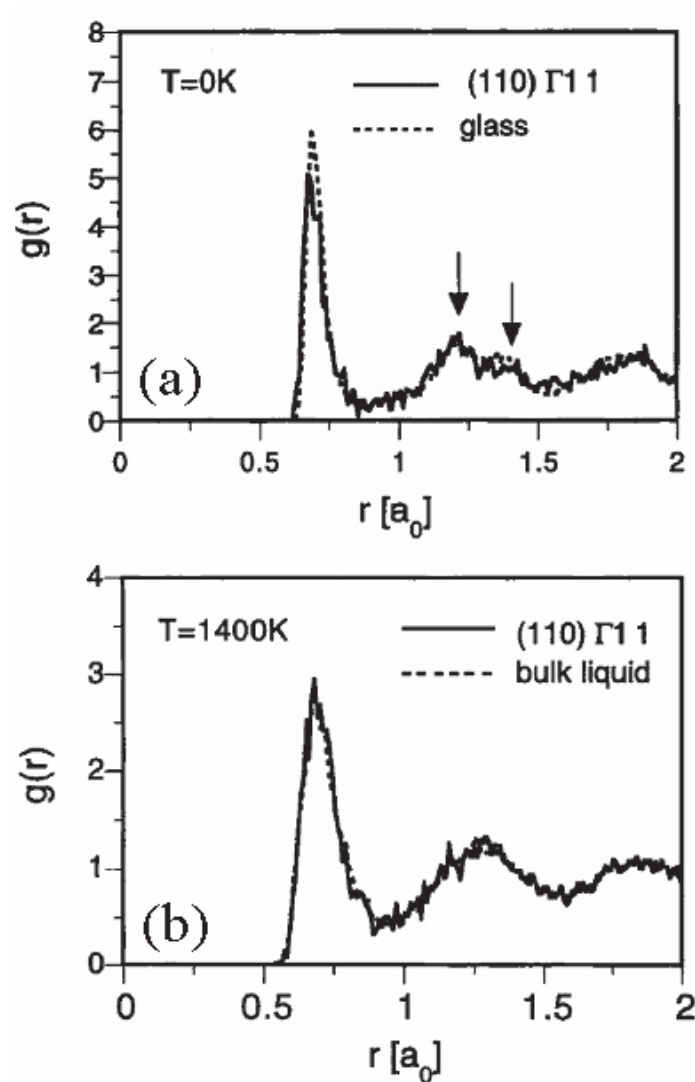
Fig. 2.7. Comparison of atomic distribution between (a) atoms in a Σ11 (θ = 50.48°) <110> twist grain boundary at 0 K and atoms in glass; (b) atoms in the same boundary but at 1400 K and atoms in a bulk liquid. The distribution is quantified by the radial distribution function g(r). The arrows in (a) indicate the split second peak. (after [5])
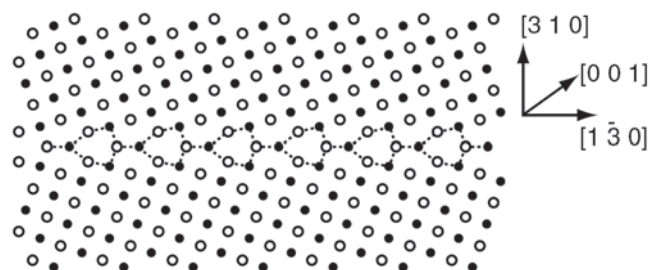
Fig. 2.8. Atomic structure of a 36.87° symmetric <100> tilt grain boundary in Cu at 0 K. The filled and open circles represent atoms locating in alternating (200) planes. The kite-shaped structural units are outlined. (after [10])

2.2 Grain boundary migration

The migration of a GB, resulting in the growth of one grain at the expense of the shrinking neighbor, is extensively involved in various processes. For example, during thermal processing of conventional industry alloys, GB migration contributes to recrystallization and grain growth. The rate of GB migration determines the kinetics of these phenomena and therefore is responsible for the evolution of microstructures, which are known to be relevant to many material properties. As demonstrated by various experiments, GB migration velocity v is proportional to a driving force p in units of J/m^3 (in dimension, identical to pressure):

$$v = mp \qquad\qquad (2.1)$$

where m is referred to as GB mobility. This proportionality can be accounted for by reaction rate theory. Assuming that atoms need only one jump to move across a GB of thickness w, the velocity is therefore a function of the difference between jump frequencies Γ_+ and Γ_- in opposite directions, and reads

$$v = w(\Gamma_+ - \Gamma_-) \qquad\qquad (2.2)$$

As schematically shown in Fig. 2.9, if the Gibbs free energy for atoms on the two sides of a GB differs by pV, where V denotes the average volume involved in those jumps, atoms tend to more likely move from grain 1 to grain 2. With the assumption that the attempting frequency ω of jumps is the same for all atoms, Eq. (2.2) then can be written as

$$v = w(\omega e^{-\frac{G_m - pV}{k_B T}} - \omega e^{-\frac{G_m}{k_B T}}) \qquad\qquad (2.3)$$

where G_m denotes the free energy barrier for atoms moving from grain 2 to grain 1, k_B the Boltzmann constant and T the temperature. Taking advantage of the Gibbs function, the velocity then reads

$$v = w\omega e^{\frac{S}{k_B}} e^{-\frac{H}{k_B T}} (e^{\frac{pV}{k_B T}} - 1) \qquad\qquad (2.4)$$

where S and H are the activation entropy and enthalpy, respectively. In reality, especially for experiments on mobility measurement in well-defined bicrystals [11], the driving force is usually small, such that $pV \ll k_B T$ and, therefore

$$e^{\frac{pV}{k_B T}} \approx \frac{pV}{k_B T} + 1 \qquad\qquad (2.5)$$

We then obtain the proportionality as

$$v = \omega e^{\frac{S}{k_B}} \frac{wV}{k_B T} e^{\frac{-H}{k_B T}} p = m_0 e^{\frac{-H}{k_B T}} p = mp \qquad \text{(2.6)}$$

and

$$m_0 = \omega e^{\frac{S}{k_B}} \frac{wV}{k_B T} \qquad \text{(2.7)}$$

where m_0 is the preexponential factor.
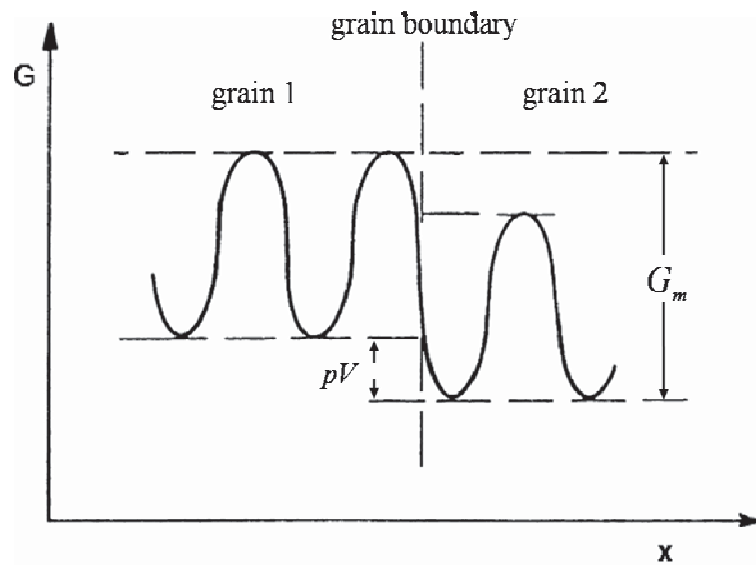
Fig. 2.9. Schematic of free energy change for atoms crossing a grain boundary with a driving force p. G_m is the energy barrier for atoms moving from grain 2 to grain 1.

2.3 Review of grain boundary migration mechanisms

Despite the importance of GB migration, its atomistic mechanism regarding how atoms move so as to alter their crystalline orientations during boundary migration is still poorly understood. To date, many mechanisms based on both experiments and MD simulations have been proposed. These mechanisms however in many cases contradict each other; each of them can be merely applied to exclusive cases under certain conditions. There is virtually no mechanism which is capable of accounting for various GB migration processes comprehensively.

Based upon the features in atomic movement during boundary motion, the existing mechanisms of GB migration can be classified into two categories, namely diffusional and

displacive mechanisms. GB migration is widely thought to be correlated to different types of diffusion owing to the fact that the activation enthalpies of the two processes in many cases are comparable. For instance, bicrystal experiments in high-purity metals [12-17] exhibited that the activation enthalpies of GB migration for low-angle GBs and high-angle GBs were consistent with the activation parameters of lattice diffusion and GB diffusion, respectively. During the annealing of cold-worked high-Mn steels, the measured activation enthalpy of GB migration involved in recrystallization was found to agree with the one of GB diffusion [18]. Huang and Humphreys [19, 20] determined the activation enthalpies of GB migration during the annealing of Al polycrystals. The measured values were found to approach the activation enthalpy of lattice diffusion. By contrast, such an agreement was rarely found in MD simulations. In recent MD simulations of grain growth by Yamakov et al. [21], GB migration nevertheless was implied by the authors to be related to GB diffusion by the agreement of activation enthalpy. In the light of the extensively reported correlation, some early GB migration mechanisms were proposed. These mechanisms tacitly considered that GB migration is realized by long-range diffusional atomic motions. Mott [22] suggested that GB migration is realized by the diffusion of a group of atoms (island) in a GB. The atom group melts from one side of a given GB, moves across the GB and solidifies to the other side of the GB. Gleiter [23, 24] described a GB as a thick layer of two interfaces between the GB and grains. In this sense, the interface is composed of kinks, ledges and terraces. During GB migration, a flux of atoms detaches from the kinks or ledges, traverses over the terraces and attaches to the steps on the opposite side. Although the two proposed mechanisms are capable of explaining many experimental phenomena, the detailed diffusional atomic motions involved have still not been validated.

For the displacive mechanisms, the corresponding atomic movements are highly ordered with specific directions and magnitudes, and therefore not relevant to diffusion. These mechanisms, usually demonstrated by both experiments and MD simulations, comprise the collective atomic motion [25-32], the shuffling [25-27, 33], the coupling [10, 34-49] and the GB migration by the motion of secondary grain boundary dislocations [50, 51].

The collective atomic motion mechanism found for high-angle GBs refers to a process in which a group of atoms move cooperatively to transform from one orientation to the other. Zhang et al. [29-32, 52] simulated the motion of asymmetric tilt GBs driven by an elastic energy difference in two grains resulting from biaxial strain application to a bicrystal. The

authors determined string-shaped collective atomic motion during GB migration. Babcock and Balluffi [25] used in situ transmission electron microscopy to study curvature-driven GB migration in thin Au films. The authors proposed a four-atom shuffling (equivalent to end-to-end string-shaped collective motion of four atoms) mechanism to rationalize their experimental observations on the migration of near-Σ5 GBs. The four-atom shuffling mechanism was later observed to participate in the migration of <100> twist GBs in MD simulations [26-28, 33].

The coupling mechanism is referred to the case that GB motion along its normal is coupled to a motion of the two grains relative to each other along the GB, i.e. grain translation for tilt GBs and grain rotation for twist GBs. This mechanism was recently suggested from theory by Cahn and Taylor [35] to be active in most cases of GB motion. Later it was verified by both MD simulations [10, 34, 37-40] and experiments [41-43]. All these studies commonly employed a shear perpendicular to both a GB normal and a boundary rotation axis as a driving force to study the motion of tilt GBs in bicrystals. It was found that the coupled boundary motion was implemented by the distortion and rotation of certain structural units (comprising the GBs) that are typically of several atoms [10, 37]. The coupling extent for tilt GBs, defined as a factor β equal to the length ratio of grain translation to GB migration, was predicted purely based on GB geometry [10, 37]. The predicted β values for various tilt GBs in both face-centered cubic (fcc) and hexagonal close-packed (hcp) metals were found to be consistent with the ones measured in experiments [41-43] and MD simulations [10, 37-40]. Recently, in response to external stress, grain growth at low temperatures, e.g. room temperature (RT), was observed in fine-grained [46] and nanocrystalline [44, 45, 47, 48] metals. The GB motion involved was thought to proceed by the coupling mechanism. Nevertheless, those experiments usually revealed smaller coupling factors than predicted. As noted by Cahn and Taylor [35], the difference in microstructures probably gives distinct coupling behaviors. For a bicrystal with a flat GB as used in many simulations [10, 34, 37-40] and experiments [41-43], the coupling readily occurs. While for complex-structured polycrystals, the coupling turns to be greatly suppressed by structural constraints. The effect of structural constraints on the coupling was later partially verified by MD simulations [49]. In Bernstein [49], the coupling was shown to be evidently blocked by some imperfections in several relatively complicated microstructures. These microstructures however confounded further analyses to discriminate the specific roles of imperfections on the inhibition of the coupling.

Pond and Smith [50] described GB migration as the motion of SGBDs with burgers vectors of DSC lattices. This mechanism can also be classified into the displacive category. It was later supported by experiments on stress-induced boundary motion in thin Au films which, interestingly, provided evidence of the coupling mechanism at the same time [51].

2.4 Review of grain boundary mobility simulation

Major efforts have been made in the past to experimentally determine the GB mobility. Owing to the complicated geometry of a GB with 5 geometric degrees of freedom (without consideration of the translation vector) it is however very difficult to comprehensively measure the GB mobility. Therefore, the computer simulation of GB migration by molecular dynamics (MD) has been developed in the past 15 years as reviewed recently by Mishin et al. [53], and detailed in [9, 27-32, 40, 52, 54-71]. Remarkable discrepancies however are found between experiments and simulations. The simulated mobilities were always found to be much larger than experimental ones, e.g. the mobilities obtained in high-purity bicrystalline experiments [12, 13, 15-17, 41-43, 72-88], by several orders of magnitude. This drastic discrepancy is usually attributed to the absence of impurities in simulations, which, to date, merely concern pure metals. The impurity inevitably existing in real materials is expected to segregate in GBs, which can retard GB motion significantly. Another discrepancy lies in that, in comparison with experiments, the simulated mobility is frequently found to be a weak function of temperature. In most simulations, boundary motion was found to be thermally activated. The computed activation enthalpies nevertheless are profoundly smaller than the ones determined in experiments. In the other cases, athermal GB motion was observed: changing temperature didn't affect mobility, or even provided temperature dependences in opposition to expectance.

In the following, we review previous MD simulations based on different driving force types. Special emphases are given to simulation conditions (e.g. driving force value, temperature and microstructures), the v-p relation, the occurrence of athermal boundary motion and the misorientation effect on mobility. At the end of this section, a short summary of the current state of GB mobility simulation is given.

Curvature-driven method

During grain growth, GBs migrate with a driving force derived from the free energy change due to the reduction of boundary area. Inspired by this idea, MD simulations were firstly performed in two dimensions by Upmanyu et al. [56, 57] and later extended to three dimensions by Zhang et al. [60]. All three studies concerned the motion of curved high-angle <111> tilt GBs, which represent an interface of a half-loop-shaped bicrystal. Owing to the inherent limit of MD timescale, the curvature κ of the built GBs has to be very large, usually in the scale of 0.5×10^8 m^{-1}. The resulting driving force p = Γκ (Γ denotes the GB stiffness with a typical value of 1 Jm^{-2}. Its exact magnitude is hard to determine [53]) became greater than 100 MPa, which is unlikely to occur for conventional alloys of micrometer-sized grains. Through varying the GB curvature, a nonlinear relationship between v and p was actually found. The authors didn't account for the nonlinearity, but simply supposed that v was proportional to p in the low driving force limit (~ 150 MPa). The reduced GB mobility m* = mΓ was then calculated by v/κ.

There are some disadvantages inherent to the curvature-driven boundary motion. Firstly, it is inconvenient to vary the driving force. For each driving force value, one has to construct a different simulation cell. Secondly, since the GBs studied are curved, one can only determine the average reduced mobility of GBs of a number of inclination angles. It is not possible to obtain the motion behaviour of a GB of specific geometry. Finally, due to the excess volume associated with a GB, the decrease in GB area leads to vacancy generation and emission from GBs, and thus very likely induces vacancy drag on boundary motion. This complicates these studies, causing additional difficulties to understand the intrinsic boundary motion behaviour.

Strain-driven method

On account of crystallographic anisotropy, the application of an external strain to polycrystalline materials may cause grains of distinct orientations to possess dissimilar elastic energy density. The energy density gradient across a GB then acts as a driving force for boundary motion. In previous MD studies, a biaxial strain parallel to a flat boundary plane was exerted on bicrystals. The requirement of elastic anisotropy in the two grains restricts the GB type to twist [27, 28, 54] and asymmetric tilt [52, 59] GBs. During GB migration, the area of studied GBs remains constant, without yielding any vacancy. The strain-driven technique therefore enables one to gain the intrinsic boundary motion behaviours

Schoenfelder et al. [27, 28, 54] employed the strain-driven method to investigate the motion of a set of twist GBs including both low-angle and high-angle GBs. The twist GBs were achieved by setting two grains in one simulation cell. By applying 3-dimentional periodic boundary conditions, the constructed microstructure denoted a layered polycrystal. The applied driving force ranged from about 20 to 100 MPa. It was found that the boundary migration velocity was approximately proportional to the driving force (note that, with 3-4 driving force magnitudes within the mentioned range, a nonlinear v-p relation was actually present, especially at low temperature, but the authors disregarded this and roughly fitted the v-p data by a straight line). In a wide temperature range from 0.48 to 0.80 T_m (T_m is the melting temperature of the material as described by the MD potential used), low-angle GBs were always observed to move faster than high-angle GBs. For low-angle GBs, their motion was found to be almost not thermally activated, which gave rise to no (or zero) activation enthalpy. Zhang et al. [52, 59] simulated the motion of a high-angle asymmetric <100> tilt GB of various inclination angles. In Zhang's studies, a similar simulation cell to the one constructed by Schoenfelder et al. [27, 28, 54] was employed. Nevertheless, periodic boundary conditions were only active along GB plane, hence the built microstructure rather stood for a bicrystal. The simulation results evidently revealed a nonlinear v-p relation, when the applied driving force varied from about 10 to 40 MPa. Given the nonlinearity, the authors suggested that the mobility is uniquely defined in the low driving force limit:

$$m = (\frac{\partial v}{\partial p})_{p \to 0} \qquad\qquad\qquad \textbf{(2.8)}$$

In addition, it was also found that the inclination angle significantly influenced both the mobility and the activation parameters.

One disadvantage associated with the strain-driven method is that it can be only applied to certain GBs. Another minor disadvantage lies in the fact that the magnitude of the driving force is not directly known. Many factors, such as GB type, temperature and the magnitude of applied strain, affect the driving force due to non-linear elastic effects. For every simulation, the effective driving force needs to be evaluated through integrating the product of internal stress and strain tensors. This causes additional computational burden.

Artificial driving-force method

The essence of a volumetric driving force is the different free energy density between grains. To mimic this, one can artificially alter the potential energy of atoms depending on their grain

affiliation. Following this idea, a crystal-orientation-dependent driving force (COD-DF) was proposed by Janssens et al. [69] and Schoenfelder et al. [28], separately. This method makes use of the orientation of an atom's neighborhood to define the belonging of an atom to distinctly oriented grains and GBs. Different energy levels are then artificially assigned to the atoms based on their belongings. The energy difference of atoms in distinct structures is subsequently exploited to provide a driving force active on atoms. Compared with other methods, the COD-DF method possesses several advantages. This method is adaptive to arbitrary boundary geometries: flat or curved; symmetric or asymmetric. The driving force is also easy to control. For an unchanged simulation cell, the magnitude of driving force is readily tuned in a wide range by variation of the artificially added energy.

With the COD-DF, Janssens et al. [69] focused on the migration of both tilt and twist GBs, present in the layered polycrystalline microstructure, at $0.85T_m$. By exerting a driving force of either 122 or 244 MPa, and assuming a proportional v-p relation, the boundary mobility was calculated. Surprising simulation results were obtained as <111> twist GBs migrated drastically, whereas all previous MD simulations had always shown that these GBs are fairly immobile. The discrepancy may result from an inappropriate construction of the simulation cell, implied by the occurrence of vacancies [69]. Suitable bicrystalline microstructures were later utilized by Olmsted et al. [9, 70]. In the latter study a great number of GBs (388 GBs) were considered. With several large driving forces (> 75 MPa) and the assumption of v-p proportionality, the computed mobilities at $0.90T_m$ [70] indicated that low-angle GBs migrated much faster than high-angle GBs. Through changing temperature, athermal boundary motion was determined for some GBs. Their mobilities remained unchanged or even decreased with increasing temperature.

Random walk method

It is known that a flat GB may fluctuate at high temperatures due to thermal effects. The boundary shape evolution resembles a random walk. This process is expected to follow the kinetic laws of one-dimensional diffusion. The GB mobility can therefore be determined from the "diffusion coefficient" of the GB, when it is treated as a particle of a one-dimensional random walk. Since the random walk method doesn't require any driving force, the obtained mobility in the zero-force limit is believed to be associated with the intrinsic boundary motion. Owing to the nature of the method, it is expected to be readily extendable to alloys, including

the effect of impurity on boundary motion. Nevertheless, the requirement of a rough boundary structure confines the method to high-angle GBs and very high temperatures.

Using this method, Trautt et al. [67, 71] performed simulations with two MD potentials on a 38.2° <111> tilt GB for several metals. The studied GB was set in a layered microstructure. It was found that the calculated mobility was sensitive to potential type, i.e. the accuracy of interatomic interactions. The computed mobilities were found to be significantly larger than the ones obtained with the strain-driven method.

GB motion during recrystallization

During recrystallization, GBs migrate with a driving force originating from a dislocation density difference between grains. Correspondingly, Godiksen et al. [62, 65] designed a bicrystalline simulation cell, in which one grain was set to be dislocation free and the other to be of variable dislocation density. When the effective driving force changed from 50 to 160 MPa, either a proportionality or a nonlinear v-p relation was observed, depending on the particular GBs. It is noted that there were three processes coexisting in Godiken's simulations. In addition to GB migration, the interactions between GBs and lattice dislocations as well as the rearrangement of excess volume associated with absorbed lattice dislocations along boundary plane, occurred simultaneously. For the last process, it is expected that vacancy drag on GB motion plays a role when the excess volume cannot be accommodated by GBs. For these reasons, it is highly likely that these calculated mobilities differ from the intrinsic GB mobility.

Short summary of GB mobility simulations

The current state of GB mobility simulation is unsatisfactory. In fact, we only know that boundary motion can be actuated with several types of driving force. Little, which is truly comparable to experimental results, has been achieved. As mentioned in the beginning of Section 2.4, there are two overall discrepancies, i.e. the significantly larger simulated mobilities than experimental values and the weak temperature dependence of these simulated mobilities. Moreover, the v-p relation present doubtable as it is expected to be nonlinear for large driving forces according to reaction rate theory, while proportionality was frequently found or assumed in many previous simulations. There are only two studies [27, 70] which systematically explored the misorientation effect on mobility. Both however revealed that low-angle GBs moved much faster than high-angle GBs. This is in fundamental conflict with

experimental findings. In addition, some other factors, e.g. potential and driving force type, are shown to have an effect on the simulated mobility.

Chapter 3

Simulation techniques

3.1 Classical molecular dynamics

Classical molecular dynamics (MD) is a simulation method based on classical mechanics. It simulates the dynamics of a many-body (particles or atoms) system with high temporal and spatial resolution. Owing to these reasons, MD allow one (and have been proved to be effective) to study the atomic-level behaviours of GBs at different temperatures. Due to the complexity of a many-body problem, a typical MD simulation however is inherently limited to thousands of particles within a simulation period up to hundreds of nanoseconds.

3.1.1. Physical basics

Based on quantum mechanics, a system of interacting atoms consists of nuclei and electrons which interact with each other. In the Born-Oppenheimer approximation (via realizing that nuclei are much heavier than electrons), the system can be thought to have nuclei at fixed positions when the electrons are considered. In this sense, the overall wavefunction for a

system can be factorized as a product of a nuclear part Ξ and an electronic part Φ. For a system of N atoms, the Hamiltonian reads

$$H = \sum_{i=1}^{N} \frac{p_i^2}{2m_i} + H_{el} \qquad (3.1)$$

where the first term on the right side concerns the nuclei, and the second term all interactions between electrons themselves and between electrons and nuclei. m_i and p_i denote the mass and the momentum of a nucleus i, respectively. We then get two Schroedinger equations:

$$H_{el}\Phi = \mu\Phi \qquad (3.2)$$

and

$$(\sum_{i=1}^{N} \frac{p_i^2}{2m_i} + \mu)\Xi = E\Xi \qquad (3.3)$$

Eq. (3.2) accounts for all electronic effects with the assumption of fixed nuclei. The eigenvalue μ represents the interatomic potential energy which in simple systems without significant covalent bonding, e.g. many close-packed-structured metals, approximately is a function of interatomic distance r_{ij} between atoms i and j. When $\mu(r_{ij})$ is determined, Eq. (3.3) calculating the total system energy E describes the motion of the nuclei. Furthermore, for a large system, e.g. bulk metals, the Schroedinger equation Eq. (3.3) can be approximated by a Newton equation meaning that we can use classical mechanics to physically reproduce the dynamics of atoms. This is what the classical molecular dynamics (MD) simulate.

In classical MD simulations, atoms move according to Newton's law

$$f_i = m_i \ddot{r}_i \qquad (3.4)$$

where f_i denotes the force acting upon atom i, and $\ddot{r}_i$ is the second time derivative of the corresponding atomic coordinate. According to the Lagrangian equal to the overall kinetic energy $K(\{\dot{r}_i\})$ minus the overall potential energy $U(\{r_i\})$

$$L(\{r_i\}, \{\dot{r}_i\}) = K(\{\dot{r}_i\}) - U(\{r_i\})$$
$$= \sum_{i=1}^{N} \frac{m_i}{2}\dot{r}_i \cdot \dot{r}_i - \sum_{i=1}^{N}\sum_{j>i}^{N} \mu(r_{ij}) \qquad (3.5)$$

the force can be calculated as the gradient of the potential energy by

$$f_i = \nabla_{r_i} L = -\sum_{j=1}^{N} \nabla_{r_{ij}} \mu(r_{ij}) \qquad (3.6)$$

because $\nabla_{r_i} K = 0$. Since in most cases the interaction decreases rapidly with increasing interatomic distance, it is sensible to limit atomic interactions within a certain range for each atom instead of all N atoms so as to significantly accelerate the time-consuming MD simulations. This range is termed a cutoff distance. Eq. (3.5) implies that the system energy E is conserved such that Eq. (3.4) is suitable to describe atomic motions in a microcanonical ensemble, which is of constant N, E and volume V. For an isothermal-isobaric ensemble (NPT), both E and V are variable and, therefore the Lagrangian must be altered. To get desired pressure p, as suggested by Anderson [89] for a cubic simulation cell (easily extend to an orthogonal cell), V can be controlled with a virtual piston of mass Q. By using scaled coordinates $s_i = r_i / V^{1/3}$, the Lagrangian turns to be

$$L(\{s_i\}, \{\dot{s}_i\}, V, \dot{V}) = V^{2/3} \sum_{i=1}^{N} \frac{m_i}{2} \dot{s}_i \cdot \dot{s}_i + \frac{1}{2} Q \dot{V}^2 \qquad (3.7)$$
$$- \sum_{i=1}^{N} \sum_{j>i}^{N} u(V^{1/3} s_{ij}) - pV$$

And correspondingly the equations of motion become

$$\ddot{s}_i = \frac{f_i}{m_i V^{1/3}} - \frac{2}{3} \dot{s}_i \frac{\dot{V}}{V} \qquad (3.8)$$

and

$$\ddot{V} = \frac{p_t - p}{Q} \qquad (3.9)$$

where p_t is the instantaneous pressure. To control temperature T, a simple method without changing the Lagrangian is to scale atomic velocity $\dot{r}_i$ after each simulation step through

$$\dot{r}_i(scaled) = \dot{r}_i \sqrt{\frac{T}{T_p}} \qquad (3.10)$$

where T_p represents the instantaneous temperature.

While knowing the equations of motion Eqs. (3.8) and (3.9), time integration based on finite difference methods subsequently gives the evolution of the system and allows one to obtain physical quantities of interest. The integration scheme employed in this work is the four-value Gear algorithm. Based on the current state of a system at t, this algorithm firstly predicts the new state after a time step Δt (set to be 3 fs in this study) by using the Taylor's expansion:

$$r_i^p(t + \Delta t) = r_i(t) + \Delta t \dot{r}_i(t) + \frac{\Delta t^2}{2} \ddot{r}_i(t) + \frac{\Delta t^3}{6} \dddot{r}_i(t)$$

$$\dot{r}_i^p(t + \Delta t) = \dot{r}_i(t) + \Delta t \ddot{r}_i(t) + \frac{\Delta t^2}{2} \dddot{r}_i(t) \qquad \text{(3.11)}$$

$$\ddot{r}_i^p(t + \Delta t) = \ddot{r}_i(t) + \Delta t \dddot{r}_i(t)$$

$$\dddot{r}_i^p(t + \Delta t) = \dddot{r}_i(t)$$

where the superscript p denotes the predicted state. The predicted atomic positions are used to compute the force and then the acceleration $\ddot{r}_i^c$ denoted by a superscript c. This acceleration differs from the $\ddot{r}_i^p$ by

$$\Delta \ddot{r}_i(t + \Delta t) = \ddot{r}_i^c(t + \Delta t) - \ddot{r}_i^p(t + \Delta t) \qquad \text{(3.12)}$$

The difference is then taken to correct the predicted values

$$r_i(t + \Delta t) = r_i^p(t + \Delta t) + c_0 \Delta \ddot{r}_i(t + \Delta t)$$

$$\dot{r}_i(t + \Delta t) = \dot{r}_i^p(t + \Delta t) + c_1 \Delta \ddot{r}_i(t + \Delta t)$$

$$\ddot{r}_i(t + \Delta t) = \ddot{r}_i^p(t + \Delta t) + c_2 \Delta \ddot{r}_i(t + \Delta t) \qquad \text{(3.13)}$$

$$\dddot{r}_i(t + \Delta t) = \dddot{r}_i^p(t + \Delta t) + c_3 \Delta \ddot{r}_i(t + \Delta t)$$

and result in the 'real' (with acceptable errors) atom positions. The four coefficients C_{0-3} in Eq. (3.13) are called "magic numbers" (in order, set to be 1/6, 5/6, 1 and 1/3) which maximize the stability of the algorithm.

3.1.2. Grain boundary construction

To build symmetric <111> tilt GBs in an orthogonal simulation cell, a layered polycrystalline microstructure is used. Fig. 3.1 illustrates the construction of GBs, where a simulation cell contains two grains with their common rotation axis <111> parallel to the z-direction. The misorientation across the GBs is obtained by rotating the left grain and the right one in opposite directions by half the tilt angle θ. One GB is therefore located in the middle of the simulation cell parallel to the x-z plane. In order to mimic the GBs occurring in a bulk and to suppress finite size effects, periodic boundary conditions are imposed to the simulation cell along all 3 directions. These settings on one hand cause that, when an atom moves out of the cell from one side, it moves back into the cell on the opposite side. On the other hand, they also result in another GB placed at the two ends of the simulation cell along the y-direction. This side GB is of the same geometry as the central one. To avoid an interaction between the

two GBs, each grain should be initially of a sufficient thickness along y. In addition, since the resulting boundary plane is periodic, only CSL GBs can be constructed without inducing preloaded strain or any other types of imperfections, e.g. vacancies or lattice dislocations.
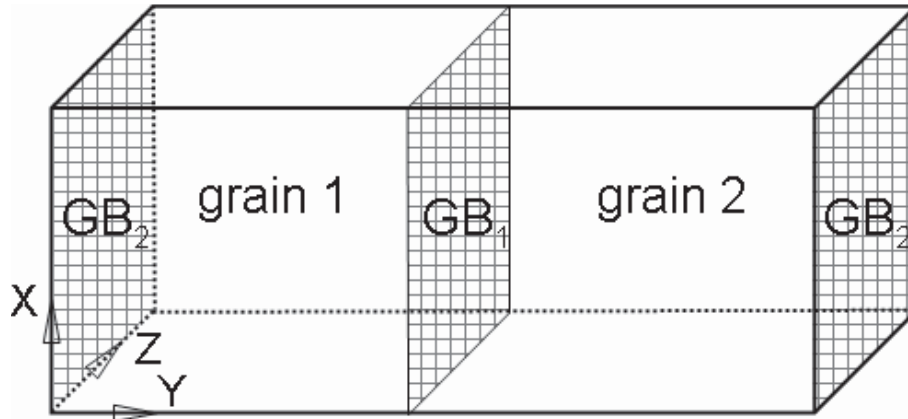
Fig. 3.1. Schematic of a simulation cell comprising two grains.

3.1.3. Interatomic potential

The performance of MD simulations highly depends on the ability of the potential μ. To describe the atomic interactions in Al, an empirical many-body potential derived from a second-moment approximation of tight-binding methods (TB-SMA) [90] is utilized together with a cutoff distance of $2.8a_0$ (a_0 is the lattice constant at 0 K). This potential, composed of an attractive term approximating the band character of metallic bonds and a repulsive term analogous to a pair potential, possesses a simple function with only a small set of adjustable parameters, thus being fairly suitable for fast simulations of a large system of thousands of atoms. Moreover, in spite of its simple function, the TB-SMA potential has been reported to well reproduce many structural and thermodynamic properties for FCC and HCP metals [90].

To further verify the performance of the TB-SMA potential, we employed the potential to estimate the melting point of Al (which was not given in [90]) with a method similar to [91]. For a high-angle <111> tilt GB of 38.21° misorientation, a simulation cell consisting of 6048 atoms was relaxed for 30 ps at different temperatures. The snapshots shown in Fig. 3.2 (visualized by Atomeye [92], which applies to all snapshots in the context) indicate that, as the temperature increases, the enhancement of disordering in the high-angle GB naturally serves as the origin for melting. When the temperature was increased from 930 K to 950 K,

the bulk regions represented by vertical lines as the projections of (111) planes disappeared completely. Hence the melting point of Al for the selected TB-SMA potential is about 940±10 K, which is rather close to the experimental value of 933 K.
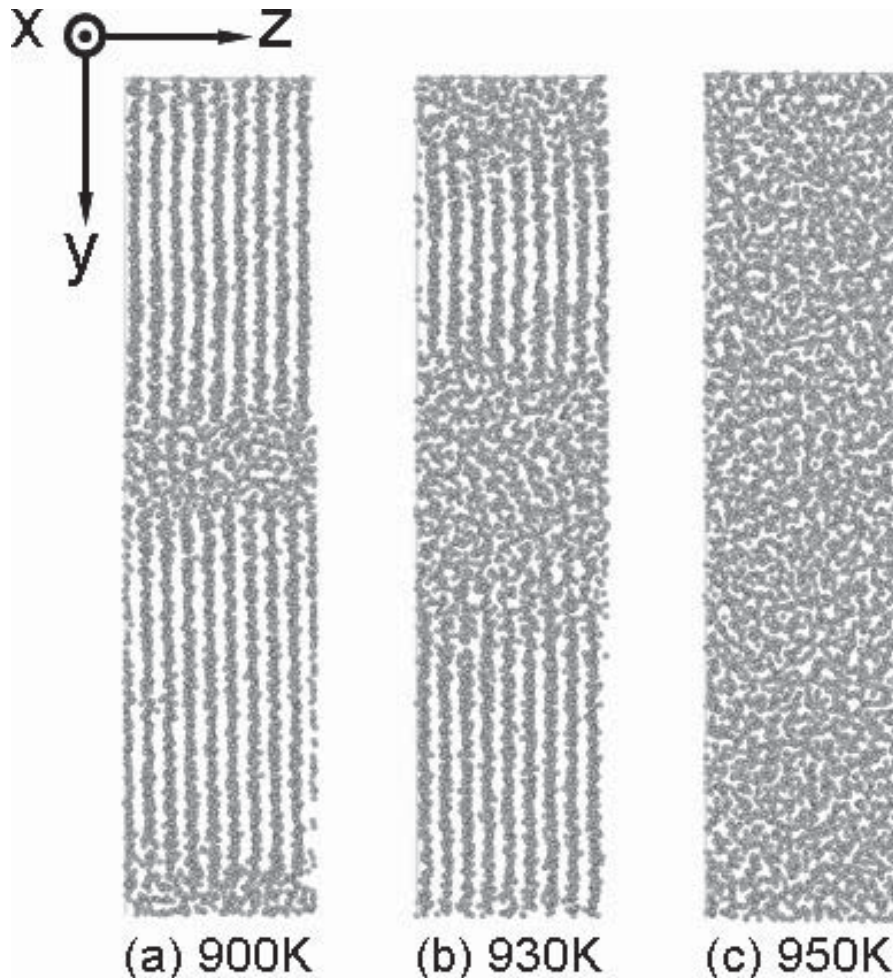
Fig. 3.2. Snapshots of relaxed layered polycrystals at (a) 900 K (b) 930 K and (c) 950 K.

3.2 Driving force

Since it is easy to control, the COD-DF is taken advantage of in the work. However, care has to be taken in the procedure of driving force application to avoid erroneous results. With the original approach [69, 70], the driving forces exerted on GB atoms seem to cause systematic errors. Low-angle GBs migrated much faster than high-angle GBs [70], whereas most experiments on recrystallization and grain growth demonstrate the opposite, i.e. real high-angle GBs are more mobile than low-angle GBs. Moreover, the simulated temperature dependence of GB mobilities was found to be rather weak or non-present in many cases [70],

whereas such behavior has never been observed experimentally. Therefore, a new formulation of the COD-DF, aiming to avoid problems found in the original approach, is introduced and assessed. In this section, we firstly analyze the limitations of the original application approach of COD-DF, and then propose a new one. Subsequently, the new approach is shown to be effective by examining the work performed by the driving force.

3.2.1 New application method of the COD-DF

In the application approach of the COD-DF used by Janssens et al. [69], the crystal orientation is quantified for each atom (local relative position to its neighbor atoms) by utilizing an order parameter, defined as

$$\xi_i = \sum_{j=1}^{12} \left| \vec{r}_j - \vec{r}_j^{X} \right| \quad (X = I \ or \ II) \tag{3.14}$$

where I and II denote the orientations of the two grains in a simulation cell. In an FCC crystal, atom i owns 12 nearest neighbors j with relative position vectors $\vec{r}_j$. $\vec{r}_j^{X}$ denotes the ideal relative vector in orientation I or II. By setting either orientation I or II as the reference, extrema of the order parameter are therefore expected to pertain to the atoms in the two grains, i.e. minima to the ones in the reference grain and maxima to the ones in the other grain. Intermediate values of ξ_i are expected to be associated with the atoms in the GB.

Nevertheless, the atoms in GBs are known to be highly disordered, especially for high-energy high-angle GBs at elevated temperatures [3]. The simple definition of the order parameter cannot account for the disordering and hence leads to serious problems. To illustrate the practical distribution of the order parameter, the simulation cell in Fig. 3.3a was segmented into layers perpendicular to y. The average order parameter per atom was then computed for each y-layer at 500 K. Fig. 3.3b displays that, as expected, small order parameter values are associated with the atoms in the reference grain, whereas large ones are assigned to the atoms in the other grain. But the atoms in the GB are highly disordered such that the order parameters are very large. To calculate ξ_i in the GB, an adjustable radius has been used to ensure that always 12 neighbors are used. In many cases the order parameters in GBs are even larger than the ones in the non-reference grain, as evidenced by the spikes of the average parameters in Fig. 3.3b. Owing to this, the structures around the atoms in the GB cannot

clearly be distinguished from those in the non-reference grain by this order parameter. In the original COD-DF formulation, both these cases would be counted as atoms inside the non-reference grain, and hence experience no driving force. Instead, some atoms inside the reference grain (but close to the GB) would have order parameters of intermediate values. Hence, these are the atoms that experience forces from the added energy in that approach. The effects of this flawed energy and force attribution are expected to be detrimental, however this is hard to quantify.
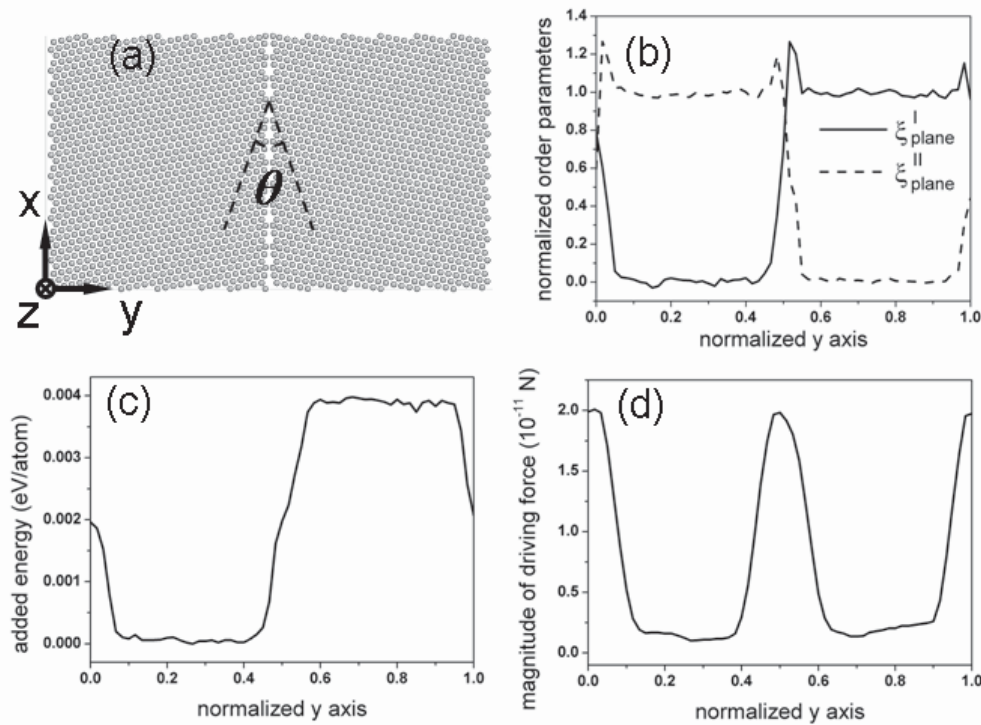
Fig. 3.3. (a) An as-built bicrystalline MD simulation cell for a <111> tilt GB with misorientation $\theta =$ 38.21°. By calculating plane-by-plane average values along the y direction, i.e. the GB normal, the distributions of (b) normalized order parameters (see text), (c) added artificial energy and (d) magnitude of driving force are plotted for a relaxed simulation cell at 500 K.

To avoid this deficiency, we propose a new approach in which every orientation is associated with its own order parameter. For the case of the bicrystal, ξ_i^I and ξ_i^{II} were assigned to the two orientations in the simulation cell respectively (Fig. 3.3b shows both their distributions along y). As a result, while the atoms in each grain can always be identified by low values of their corresponding order parameter, those atoms with both, ξ_i^I and ξ_i^{II} being high don't belong to any grain, and hence are in the GBs.

Essentially, GB migration is driven by the free energy density difference in adjoining grains. The energy change across the GB gives rise to individual driving forces on the GB atoms.

There is no way to determine these specific forces on these atoms, but fortunately, this is not required either. On the basis of classical rate theory of atoms crossing the GB, GB migration has to be considered as a drift motion. Therefore, it is conceivable that only the mean driving force over atoms across the GB is of high importance, rather than the specific driving force on each atom in the GB. In the original COD-DF, the individual forces have been defined, in respect of magnitude and direction, by calculating for each atom the derivative of the added energy. This procedure ensures a correct relation between the individual forces and the work they perform during GB motion. However, as shown above, the original definition of this energy is still flawed.

In the present approach, the first step is to define a reasonable added energy to each atom. For this we associate 3 discrete energy states with 3 distinct structures: atoms of orientation I with zero artificial energy, the ones of orientation II with energy u_0, and the other disordered atoms with $u_0/2$. The added energy on atom i then reads

$$u_i = \begin{cases} 0 & \xi_i^I < \xi_{low} \text{ and } \xi_i^{II} > \xi_{low} \\ u_0 & \xi_i^I > \xi_{low} \text{ and } \xi_i^{II} < \xi_{low} \\ u_0/2 & \text{otherwise} \end{cases} \qquad (3.15)$$

Here ξ_{low} is a threshold used to clearly recognize the belonging of an atom to either grain I or II, or to the GB, at any temperature. ξ_{low} is defined as a fraction f of the difference between the average order parameter inside the reference and the non-reference grain at a given temperature T:

$$\xi_{low}(T) = f \cdot \Delta\xi(T) \qquad (3.16)$$

$$\Delta\xi(T) = \left\langle \xi_{i\in\{non-ref.\}}(T) \right\rangle - \left\langle \xi_{i\in\{ref.\}}(T) \right\rangle \qquad (3.17)$$

The adjustable factor f is set constant to 0.4 in this study. This is similar to the original COD-DF [69, 70], in which only those atoms with their normalized parameter ξ_i in a certain fixed range were exposed to a driving force: $f < \xi_i / \left\langle \xi_{i\in\{non-ref.\}}(T=0) \right\rangle < 1-f$. In both COD-DF formulations, the threshold prevents atoms inside the grains from experiencing an unwanted driving force from thermal fluctuations. However in the original COD-DF, the belonging of atoms to either grain was systematically shifted with temperature, as $\xi_i(T)$ was compared to fixed values. The effect of this is unknown, but it may introduce a systematic temperature dependence. In the present approach using Eqs. (3.16) and (3.17), this effect is suppressed, at

least for the most part. In Fig. 3.3b, the "normalized order parameters" actually display $\xi_{plane}^{X} = (\langle \xi_{i \in \{y-plane\}}^{X}(T) \rangle - \langle \xi_{i \in \{ref.\}}^{X}(T) \rangle) / \Delta \xi(T)$. In this normalization, the criterion ξ_{low} is indicated by the fixed value f = 0.4.

Fig. 3.3c shows the added energy per atom defined by Eq. (3.15) and $u_0 = 0.004$ eV, averaged across planes parallel to the GB. This averaged energy complies with the magnitude of u_0 inside the high energy grain, as intended. Also it appears to be rather continuous across the GB, in spite of the fact that there are only 3 distinct levels of added energy.

Obviously, there is no direct way to derive individual forces from the three discrete energy levels of Eq. (3.15). Therefore, a force $\vec{F}_i$ on each atom i depending on u_i has been firstly defined and verified subsequently:

$$\vec{F}_i = -\sum_j \frac{u_i - u_j}{\|\vec{r}_j\|} \frac{\vec{r}_j}{\|\vec{r}_j\|} \tag{3.18}$$

Here, atom i is assumed to interact with its neighboring atoms j individually, in linear superposition. The forces act in radial direction (as before, $\vec{r}_i$ denotes the vector between atoms i and j), as if they were part of a simple MD pair potential. The magnitudes and signs of the forces depend on the added energies u_i and u_j, and have been defined like in a finite difference approach. The range of these forces in this study is chosen to include all neighbors inside a cutoff radius of $2.8a_0$, where a_0 is the lattice constant at 0 K. This cutoff distance includes atoms as far as the 7th neighbors. This is in deviation of earlier approaches, where only the first neighbors had been considered [69, 70]. Since the energy state u_i associated with each atom is updated every time step, the overall DF is of a stochastic nature. Fig. 3.3d illustrates that the magnitudes of the individual driving forces averaged over y layers change continuously from one grain to the other. The peaks at the locations of the GBs demonstrate that the driving forces are intensively exerted on the atoms in the GBs. Note that Fig. 3.3d only shows the average magnitudes of the driving force vectors. This average driving force curve therefore is not the derivative of the added energy curve (Fig. 3.3c).

It should be noted that a variety of other individual energy and force definitions could have been chosen, for instance based on an order parameter $\delta_i = \xi_i^I - \xi_i^{II}$ to define the added energy. This parameter δ_i refers to both orientations involved and therefore can, in principle,

distinguish between disorder in the GBs and that caused by thermal vibrations. By its definition, the average of δ_i over a y-plane is expected to be close to -1 or +1 in grain I or II, respectively, and close to zero in the GB at any temperature. However, the individual values of δ_i in the GB would strongly deviate from zero, which might cause problems. In the present study, Eq. (3.18) has been utilized, after the validation described below, since only the effective driving force on the GB is assumed to be of importance.

3.2.2 Verification of the new approach of driving force application

To test our new driving force application approach, a boundary migration simulation with added energy $u_0 = 0.004$ eV/atom, which corresponds to a driving force of about 40 MPa, was performed at 500 K for the 38.21° GB shown in Fig. 3.3a. During this simulation, the number of atoms with the same energy state was recorded every 6 ps. The number evolution of the three optional energy states was then plotted in Fig. 3.4a. In the simulation of 600 ps, the number of atoms with $0.5u_0$ (disordered atoms in GBs) only slightly varied and generally stayed at the same level. The decrease in high-energy atoms, occurring between $t_0 = 186$ ps and $t_1 = 192$ ps, therefore correlated to the increase in low-energy atoms at the same moment. By checking the distribution of added energy across the GBs, these changes were found to be associated with the migration of the central boundary in the simulation cell (Fig. 3.4b).

The evolution of energy states offers the possibility to evaluate the boundary migration velocity by normalizing the total number of states, constantly identical to total atoms, to the y axis (the direction of boundary migration). According to Fig. 3.4a, the boundary is found to migrate in a stop-and-go manner (jerky motion), as also observed in [10, 37-39]. During the waiting time, the GBs fluctuated around their equilibrium positions. In the cases of a small driving force and low temperature, this procedure could last for a long period. For example, the first plateau in Fig. 3.4a took 186 ps. By lowering the driving force to ~20 MPa but keeping the other conditions, a period of ~ 4.5 ns was found for the same GB right before its first migration. Additionally, this procedure was found to behave differently from time to time, as evidenced by the diverse lengths of two plateaus in Fig. 3.4a. This implies that the waiting times vary, as to be expected for a thermally activated process. During the short moving period ($t_0 < t < t_1$), the boundaries moved at a high speed. Fig. 3.4a and Fig. 3.4b show that the central GB migrates by about 3.3 Å, i.e. three (231) boundary planes, in an interval of 6 ps,

which equals an instantaneous migration velocity of 55 m/s. Taking this jerky manner into account, a simulation time consisting of at least several migration events is required to evaluate migration velocity with sufficient accuracy. To determine the velocity in the present study, the location of the GB was identified as described above and the position y(t) was recorded. The slope of a linear fit to y(t) was taken as the boundary migration velocity, and the deviations were taken as error bars in the following.
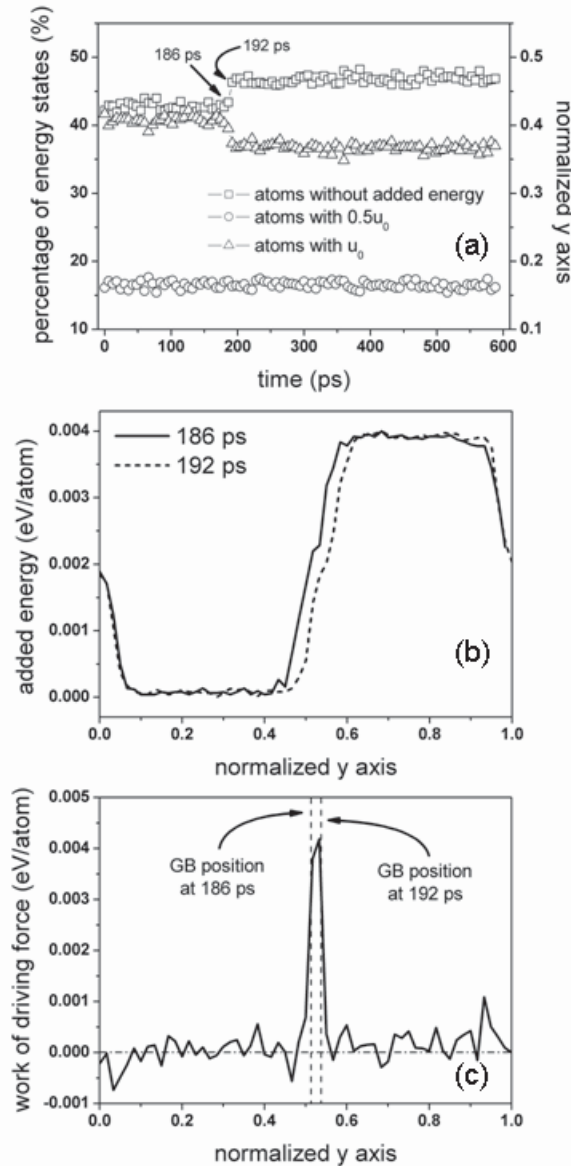
Fig. 3.4. (a) Evolution of the abundance of the three artificially imposed energy states for a <111> tilt GB with θ = 38.21° at 500 K. The numbers are normalized to show the motion of GBs as a function of time. The 2 points in time before and after migration are marked. (b) Corresponding distributions of added energy in the 2 temporal points. (c) Work performed by the driving force calculated by Eq. (3.18) during this time interval.

The work performed by the individual driving forces as defined in Eq. (3.18) can be quantified by integrating their powers over time:

$$W_i = \int_{t_0}^{t_1} \vec{F}_i(t) \cdot \vec{v}_i(t) dt \qquad\qquad \text{(3.19)}$$

Here $\vec{v}_i(t)$ is the instantaneous velocity of atom i. The work W_i was calculated using the same integrator as used for the MD simulation itself. In order to keep numerical errors low, this integration is restricted here to the time period from $t_0 = 186$ ps to $t_1 = 192$ ps, in which the GB motion actually took place. Fig. 3.4c displays W_i averaged over all y-planes along the GB normal. As expected, there is no work performed on the atoms inside the grains, where fluctuations resulting from thermal motion are averaged out. But the individual driving forces actually performed work on those atoms which altered their orientation and hence, really served as a driving force for boundary motion. Significant work of about 0.004 eV/atom has been done. This magnitude agrees very well with the artificially applied energy on each atom, which was specified to drive boundary motion. This proves that the force defined by Eq. (3.18) essentially reflects the intended energy dependence of Eq. (3.15), even though it is not the direct derivative. Moreover, it is worth mentioning that the extension of driving force ranges to more neighbor atoms in Eq. (3.18). This has been found to be important to obtain the agreement between the intended energy and the work actually performed.

Chapter 4

Migration mechanisms

To elucidate the mechanisms of GB migration, GB migration with regard to a series of <111> tilt GBs, as listed in Table 4.1, was simulated in a wide temperature range with various magnitudes of driving force. As discussed in Section 3.1.2, these GBs were constructed in a layered polycrystalline simulation cell, so that the GBs studied are not only perfectly symmetric but also of a coincidence orientation, i.e. CSL GBs (with a maximum Σ of 49). We probed GB migration at three temperatures (10 K, 500 K and 750 K). These temperatures cover a large range from 0.01 to 0.80 T_m (T_m is the simulated melting temperature) so as to enable us to explore the temperature effect on GB migration. Specifically, the three temperatures were chosen to correspond to the magnitudes either of particular theoretical significance or already studied in experiments, thus favoring comparisons. The lowest temperature 10 K ($0.01T_m$) was selected to exclude thermal effects to a large extent. Hence, the boundary motion behavior at this temperature served as a ground state. GB migration at the medium temperature 500 K ($0.53T_m$) was used to mimic the motion during low-temperature grain growth reported in fine-grained and nanocrystalline metals [44-48]. Lastly, the high temperature 750 K ($0.80T_m$) stands for a typical annealing temperature for commercial Al alloys, and therefore boundary motion at this temperature should correspond to the situation occurring during recrystallization and grain growth.

Table 4.1. The symmetric <111> tilt GBs in Al studied in this work[*]

θ (°)	GB plane	Σ	N	L_x (Å)	L_y (Å)	L_z (Å)
9.43	(10 11 1)	37	5328	34.8	121	21
13.17	(7 8 1)	19	5472	49.9	86.5	21
17.9	(5 6 1)	31	6696	55.2	95.7	21
21.79	(4 5 1)	21	4032	30.3	105	21
27.8	(3 4 1)	13	7488	71.5	82.6	21
32.2	(5 7 2)	13	5616	62	71.5	21
38.21	(2 3 1)	7	6048	52.5	90.9	21
43.57	(5 8 3)	49	7056	69.4	80.2	21
46.82	(3 5 2)	19	7296	43.2	99.9	28.1
50.56	(4 7 3)	37	7992	60.3	105	21

[*] θ, misorientation angle; Σ, the reciprocal density of coincidence sites; N, number of atoms in the corresponding simulation cell; L_x, L_y and L_z, simulation cell dimensions.

The layered polycrystals after construction were relaxed at the chosen temperatures to an equilibrium state. Subsequently, the improved application scheme of the COD-DF, as suggested in Section 3.2.1, was adopted to make GBs move. The driving force magnitude was set to vary from 1 MPa to several hundred MPa. It is noticeable that a unit of eV/atom, instead of Pa, is used frequently for the driving force because this unit doesn't vary with temperature. For Al of a_0 = 4.05 Å (a_0 is the lattice constant at 0 K set in the TB-SMA potential), 0.001 eV/atom is equal to 9.65 MPa at 0 K, which slightly decreases with increasing temperature due to thermal expansion of the lattice constant.

In order to understand how atoms move during GB migration, the evolution of atomic positions is therefore of main concern. Atomic positions/coordinates were stored with intervals from 0.3 to 3 ps, depending on the length of simulation duration. To trace atomic trajectories for boundary motion, atomic displacements were represented as vectors from the initial coordinates after relaxation pointing to the ones at a specific moment.

4.1 Results of grain boundary migration

4.1.1 Low-temperature behaviors

We firstly focus on GB motion behaviors at 10 K (0.01 T_m). Since GBs were found to remain flat during migration, the total displacement d of the two GBs in a simulation cell, being

positive if the low-energy grain grows, was measured as d = $L_y N_{low-E}/N_{total}$. L_y, N_{low-E} and N_{total} denote the simulation cell size along the common GB normal, the atoms in the low-energy grain and the total atoms, respectively. Representative temporal evolutions of the GB displacement driven by distinct driving force magnitudes are shown in Fig. 4.1. In general, the motion curves look similar for all the GBs studied. With relatively low driving forces, e.g. 0.01 eV/atom (~ 97 MPa), each GB was found to displace by a short distance, e.g. several atomic layers parallel to the GB, in the beginning of the simulation and not move any further later. By contrast, larger driving forces in a range from 0.02 to 0.03 eV/atom (specific to GBs) rendered profoundly enhanced GB motion.
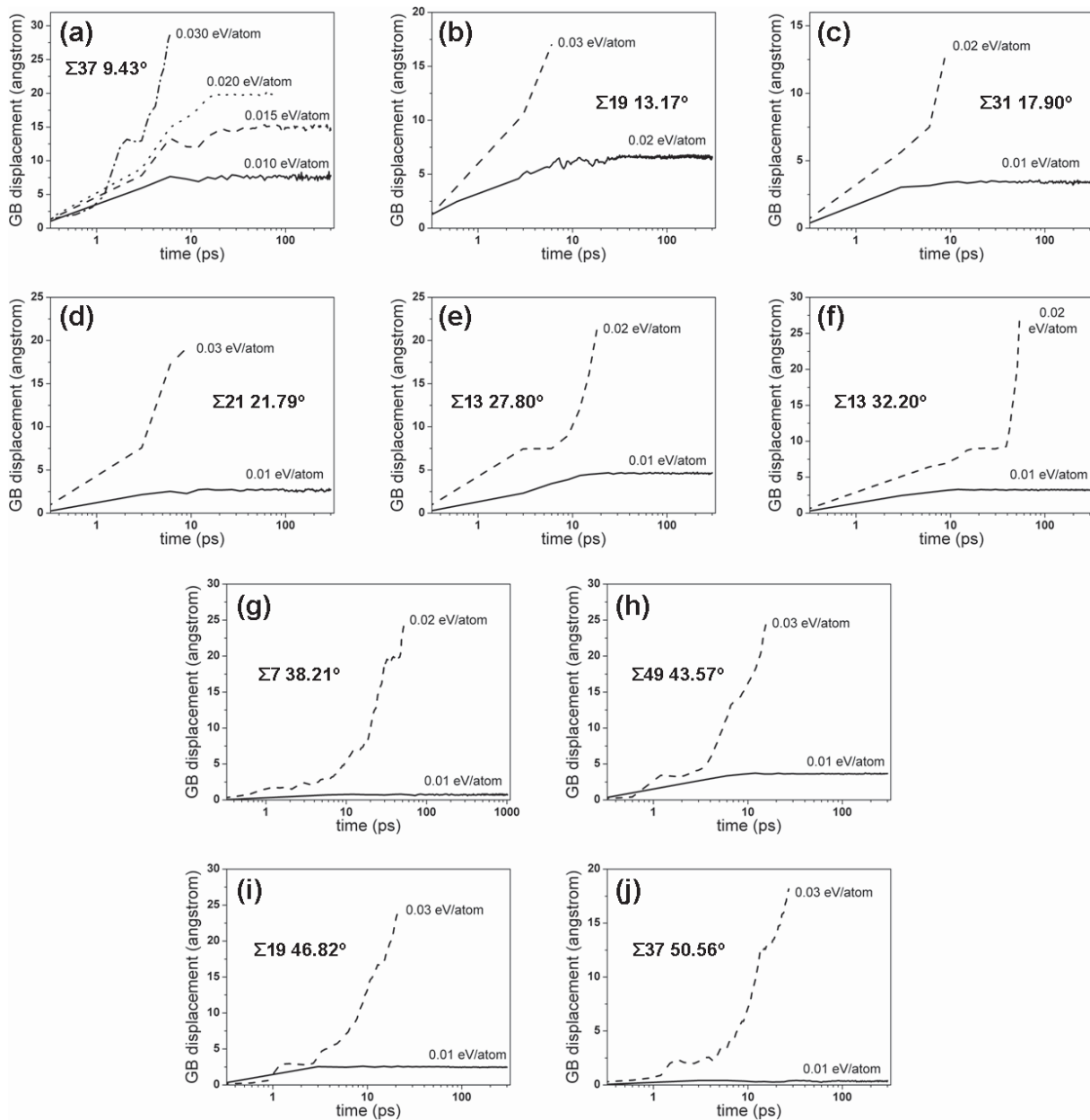

Fig. 4.1. GB displacement versus time at 10 K. The misorientation angle and the magnitudes of driving force are indicated.

The fairly limited boundary displacement in the initial stage of simulations was found to be caused by the glide of GB dislocations and their subsequent blockage. For a low-angle symmetrical <111> GB, the dislocations have a Burgers vector along the <1-10> direction. An example with respect to a 9.43° GB is given. Fig. 4.2 displays a set of snapshots concerning the motion of one single GB dislocation for the selected GB with a driving force of 0.01 eV/atom. These snapshots (and all other snapshots in this chapter) represent projections along the <111> rotation axis (note that, to clearly recognize dislocation core, only one (111) plane normal to the rotation axis is shown). The atoms in Figs. 4.2a-f are colored according to atomic coordination number: light and dark spheres represent 12 and non-12 coordinated atoms, respectively. With this coloring scheme, the dislocation core is reflected as a cluster of non-12 coordinated atoms. Fig. 4.2a refers to the initial state of the GB after relaxation. The initial GB position along the y direction is indicated by a dashed line which transverses through the centre of the dislocation core in Fig. 4.2a and serves as a reference line in Figs. 4.2b-f. During migration, the dislocation was observed to glide along a (111) plane parallel to the rotation axis, as marked by a solid line in Figs. 4.2a-f, from the upper low-energy grain side towards the lower high-energy grain side. The dislocation glide proceeded until about 9 ps (Fig. 4.2d). There was no further dislocation motion found in Fig. 4.2e at 12 ps or in Fig. 4.2f at a much later moment of 300 ps.
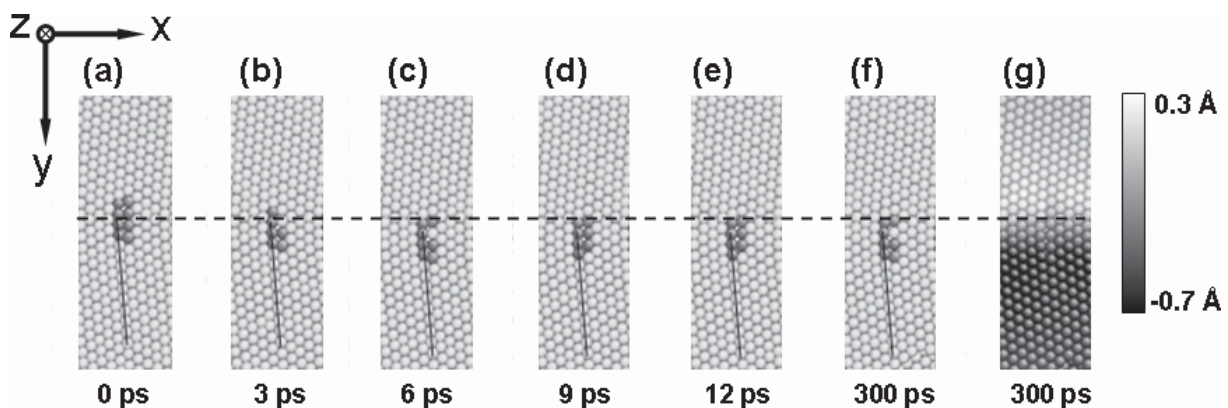
Fig. 4.2. Snapshots of the motion of a 9.43° <111> tilt boundary responding to a driving force of 0.01 eV/atom. (a-f) are colored according to atomic coordination number: light and dark spheres represent 12 and non-12 coordinated atoms, respectively. (g) is colored in accordance with the atomic displacement vectors along the x-direction. A color map with respect to the displacement vectors is given. The dashed line across (a-f) denotes the initial GB position. The solid line in (a-f) marks the same (111) plane parallel to the <111> rotation axis.

It is known that dislocation glide must be accompanied by a shear. Considering the geometry of our constructed GB, this shear is expected to occur mainly along the x direction. Fig. 4.2g provides the same snapshot as the one shown in Fig. 4.2f. But the atoms are colored in

accordance with their displacement vectors along the x direction. It is found that the atoms locating on the two sides of the boundary plane were displaced in opposite directions. This finding reveals that there is a relative translation between the two adjacent grains.

The extent of translation is quantified as the difference of average atomic displacement in the two grains and plotted as a function of time in Fig. 4.3a. For comparison, the temporal evolution of GB displacement is plotted in the same figure. According to Fig. 4.3a, GB motion is coupled to grain translation. This phenomenon represents the coupling mechanism found in previous studies [10, 34, 37-40]. Nevertheless, there are two divergences determined. The previous studies observed that, once GB migration was actuated, the motion process evolved continuously. Differing from that, GB motion in this study was however always inhibited after a short-distance movement. The predicted coupling factor β equals $2*\tan(\theta/2) = 0.165$ (θ denotes misorientation angle) for a 9.43° GB. This value is found to be remarkably larger than the values (~ 0.1) calculated from the data shown in Fig. 4.3a.
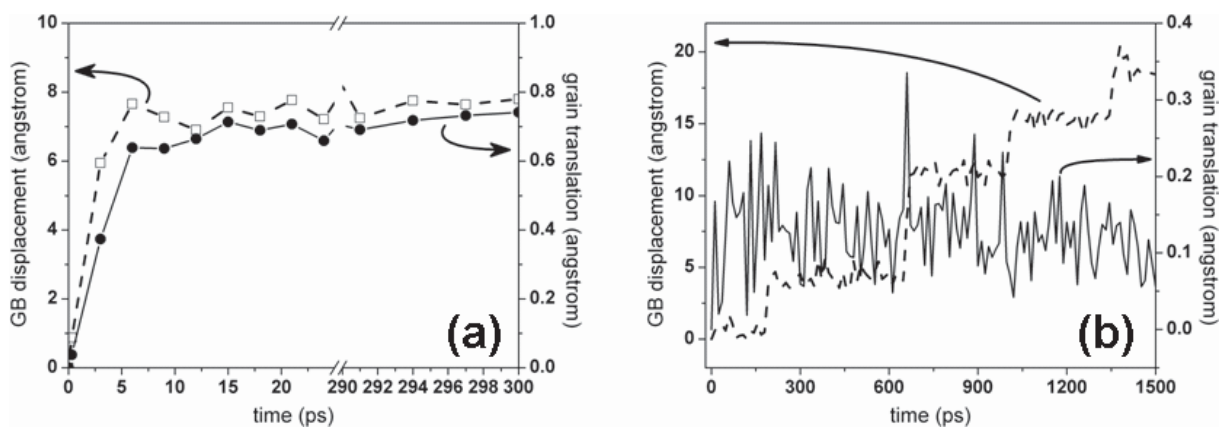
Fig. 4.3. Comparison between the temporal evolutions of GB displacement and grain translation for (a) a 9.43° GB driven by a driving force of 0.01 eV/atom at 10 K and (b) a 38.21° GB driven by a driving force of 0.004 eV/atom at 500 K.

The discrepancies in coupling behaviors found here are ascribed to distinct microstructures, i.e. bicrystals and layered polycrystals. For the bicrystals in [10, 34, 37-40], grain translation was free to proceed; macroscopic shape change was allowed to develop without impediment. Coupling of an ideal factor β consequently took place incessantly. For a layered polycrystal in this study, coupling was however restricted. To elucidate the structural effect of a layered polycrystal on coupling, a schematic depicting a projection of our simulation cell along the rotation axis is drawn in Fig. 4.4. By exerting a driving force, both GBs energetically tend to move towards the high-energy grain side. Owing to coupling, the approaching of the two GBs

gives rise to two shears (strain) in opposite directions, which obviously impede grain translation, i.e. the macroscopic shape change becomes fundamentally suppressed. The blockage of grain translation in turn prevents GB motion. In this sense, the two GBs in one simulation cell serve as structural constraints to boundary motion. The structural constraints cause the shear stress to accumulate as boundaries displace away from their initial position. At some point, the stress becomes balanced with the applied driving force (may be also assisted by the distortion of GB dislocation cores), and therefore there is only a limited GB displacement. Consequently the initial displacement increases with increasing driving force, as shown in Fig. 4.1a when the driving force varied from 0.01 to 0.02 eV/atom.
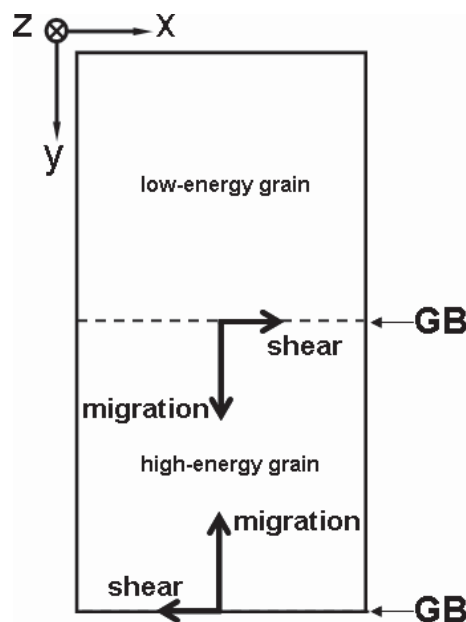
Fig. 4.4. A schematic to illustrate the suppression effect of structural constraints on grain boundary migration.

However, as the driving force reached 0.03 eV/atom, GB motion became profoundly enhanced (Fig. 4.1a). This enhanced motion behavior is attributed to the occurrence of local plastic deformations (note the term 'local plastic deformation' used in the context refers to certain deformation types which do not alter specimen shape). Fig. 4.5a shows a snapshot at 4.2 ps, which reveals that there are two blurring regions (plastic deformations) inside the lower high-energy grain. The regions marked as '1' and '2' represent a distorted dislocation core and a shear band, respectively. The shear band penetrates the high-energy grain and connects to two GBs. With a sufficiently large driving force, the accumulative shear stress from the coupling effect became large enough to trigger plastic deformations, which in turn accommodated the shear and permitted further GB migration.
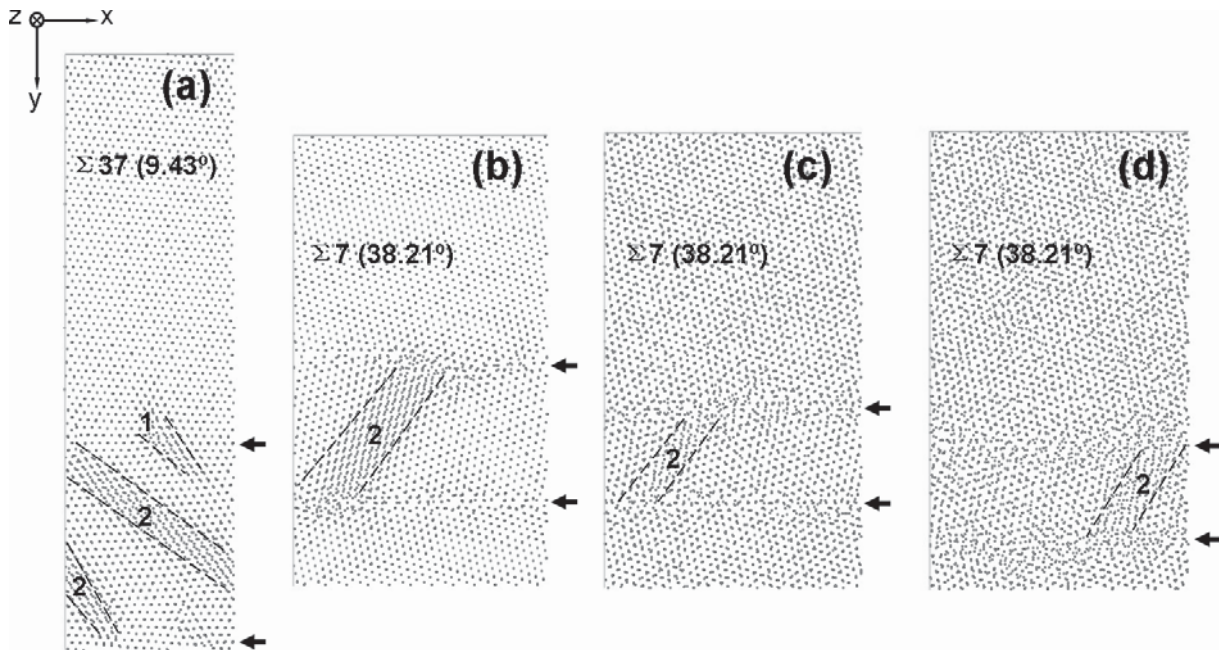
Fig. 4.5. Local plastic deformations occurring during the motion of (a) a 9.43° GB with a driving force of 0.03 eV/atom at 10 K, a 38.21° GB with a driving force of (b) 0.02 eV/atom at 10K, (c) 0.02 eV/atom at 500 K and (d) 0.03 eV/atom at 750 K. Snapshots (a-d) were obtained at 4.2, 30, 9 and 30 ps, respectively. The snapshots share a common coordinate system shown in the upper-left corner. The blurring regions, marked with dashed lines, represent either the distortion of GB dislocation core as '1' in (a) or shear bands as '2' in (a-d). The arrows point to the positions of the two GBs.

The above descriptions of a low-angle boundary motion subjected to a variety of driving force magnitudes exactly apply to all the GBs studied (Figs. 4.1a-j). However, for high-angle Σ GBs, boundary migration turns to be implemented by the glide of dislocations of multiple Burgers vectors consisting of CSL vectors, instead of one single family of dislocations for low-angle GBs. Fig. 4.6a shows a snapshot at 24 ps for the motion of a 38.21° Σ7 GB driven by a driving force of 0.02 eV/atom. In this case, the GB initially placed at the edge of the SC underwent a significant migration by about 12 Å, while the central GB roughly held its position. The displacement vectors for the atoms which altered their orientation due to the edge GB migration were analyzed. A rectangular sub-region marked in Fig. 4.6a is magnified and shown in Figs. 4.6b-e with distinct coloring schemes. The atoms in Figs. 4.6b-d are colored according to their displacement vectors along the x, y and z directions, respectively. In Fig. 4.6e, the atoms are colored in accordance with the magnitudes of displacement vectors in the x-y plane. For each figure, a specific color map is added.
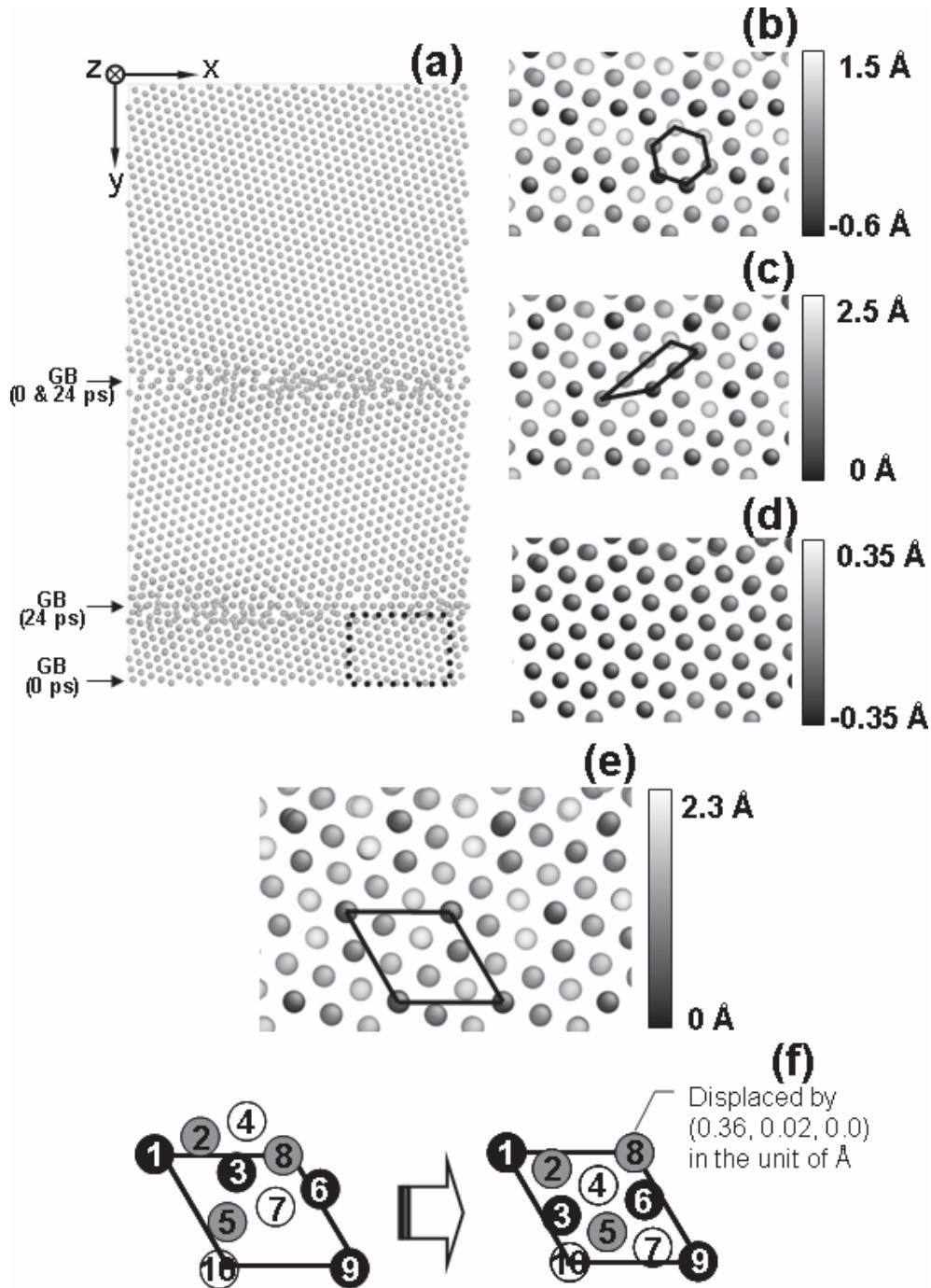
Fig. 4.6. (a) A snapshot for the migration of a 38.21° Σ7 <111> tilt GB driven by a driving force of 0.02 eV/atom (about 193 MPa) at 10 K. The atoms are viewed along the <111> rotation axis, i.e. the z direction. The arrows in (a) point to the positions of the two GBs at 0 and 24 ps. A sub-region, marked by the rectangle, consists of some atoms which varied their orientation due to the migration of the edge GB. The sub-region is enlarged and shown in (b-e) with distinct coloring schemes. The atoms in (b-d) are colored according to their displacement vectors along the x, y and z directions, respectively. The atoms in (e) are colored in accordance with the magnitudes of displacement vectors in the x-y plane. For each coloring scheme, a specific color map is offered. The added polygons in (b, c, e) serve to indicate some repeating displacive units. The atoms included in the unit in (e) are drawn schematically in the right part of (f). These atoms are indexed and colored according to the 3 sequentially stacking (111) planes. The initial positions of these atoms at 0 ps are given in the left part of (f).

There are several features found in Fig. 4.6. First, the atoms moved as far as 1.5, 2.5 and 0.35 Å along the x, y and z directions, respectively (see Figs. 4.6b-d). The atomic movements therefore occurred within the (111) planes normal to the rotation axis, rather than along the rotation axis. Since the (111) interplanar spacing in Al is about 2.3 Å, there was therefore no atom exchange among these (111) planes. Secondly, Fig. 4.6e shows that the magnitudes of displacement vectors within the (111) planes were well below 2.3 Å. This value is smaller than the nearest atomic distance $r_0 = 2.8$ Å in Al, thus these atomic movements are not relevant to diffusion. Finally, the distributions of displacement vectors in the x and y directions as well as the displacement magnitudes in the x-y plane, were all fairly regular. Some repeating patterns, hereafter termed displacive units, are drawn in Figs. 4.6b, c and e. We notice that the displacive unit in Fig. 4.6e represents the CSL lattice for the Σ7 GB. Hence, the displacive unit must be formed by the glide of the multiple GB dislocations.

To get more details about how atoms alter their orientation during GB migration, the 10 atoms included in the parallelogram-shaped displacive unit shown in Fig. 4.6e are indexed and drawn schematically in the right half of Fig. 4.6f. It is found that the 10 atoms are situated on 3 sequentially stacking (111) planes (the featured stacking for fcc crystals). To facilitate description, we designate the atoms in black, grey and white to the first, second and third (111) planes, respectively. The initial positions of these atoms relative to the displacive unit are depicted in the left half of Fig. 4.6f. During migration, relative to the atom 9, the atoms 3 and 6 on the first plane rotate equally in an anticlockwise direction. By contrast, relative to the atom 1, the atoms 3 and 6 rotate to a distinct extent in a clockwise direction, thus yielding distortion. For the three atoms on the second plane (grey), there is only a pure rotation around the atom 8. For the three atoms on the third plane (white), except for rotation and distortion, the atom 4 leaves its initial environment and turns to be a new nearest neighbor of atom 10. It should be noted that the initial atomic positions are not spatially repeatable. We therefore suggest that there must be other distributions of atoms which results in the same displacive unit. In total, it is concluded that the Σ7 GB migrates through collective motion of a group of atoms in a rather concerted manner, which is essentially equivalent to the concurrent glide of multiple GB dislocations. It should be noticed that during GB migration the four corner atoms indexed as 1, 8-10, move mainly along the x direction. The x-direction displacement indicates a shear resulting from the glide of GB dislocations. The shear was found to increase as the GB migrated. Eventually, a shear band was formed, as illustrated in Fig. 4.5b.

The glide of multiple GB dislocations through collective atomic motion, discussed for the Σ7 GB, was observed to hold for the other high-angle Σ GBs (Table 4.1) as well. With a large driving force from 0.02 to 0.03 eV/atom, CSL-shaped displacive units were always observed for these GBs, as drawn schematically in Fig. 4.7 with the same coloring scheme as Fig. 4.6f.
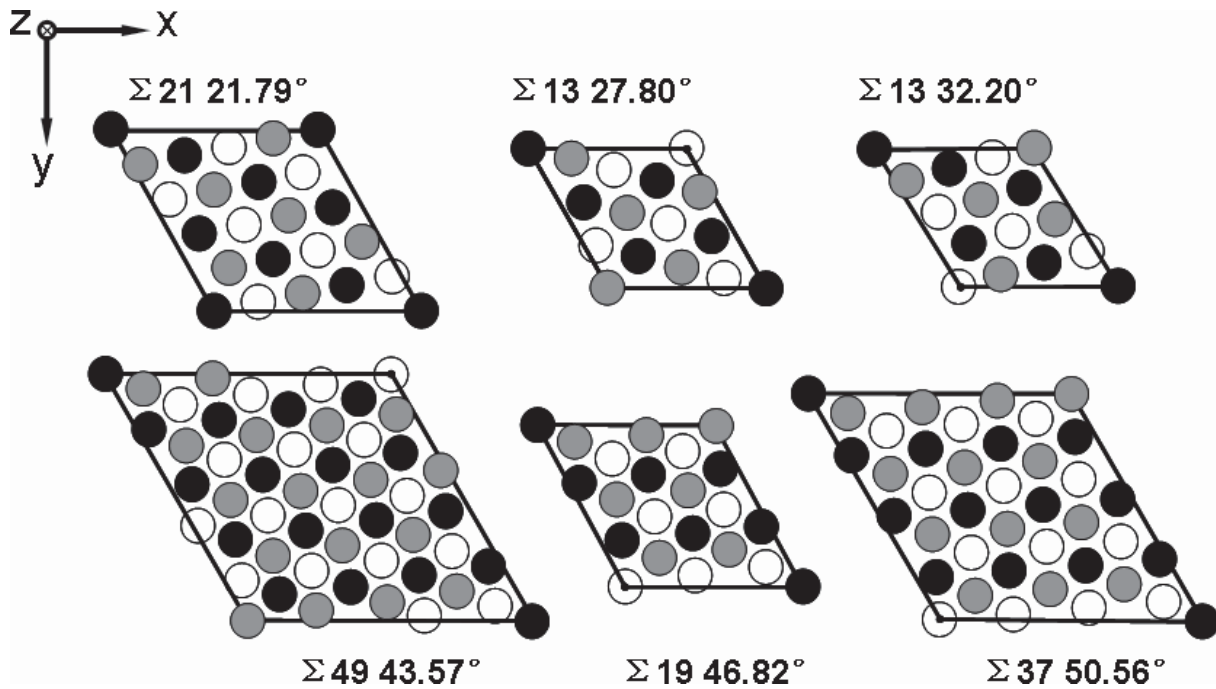
Fig. 4.7. Displacive units for high-angle Σ GBs. The Σ value and the misorientation angle for each unit are given.

4.1.2 Medium-temperature behaviors

GB migration was next investigated at a medium temperature of 500 K (0.53 T_m). At this temperature, the mechanisms of GB migration remained unchanged as the ones at 10 K. GBs migrated through GB dislocation glide. The glide of multiple GB dislocations for those high-angle Σ GBs led to some CSL-shaped displacive units. Nevertheless, owing to thermal effects, some new motion features occurred.

Fig. 4.8 shows the GB displacement vs. time curves obtained at 500 K. Concerning the six GBs with misorientation angles of up to 32.20° (Figs. 4.8a-f), the thermal effects lay in inducing strong fluctuation of the GB position. In addition, it is interesting to find that, for the 17.90° GB, a driving force of 0.02 eV/atom, which produced the enhanced boundary motion at 10 K (Fig. 4.1c), caused only a limited displacement at 500K (Fig. 4.8c). Fig. 4.8c displays

that a larger driving force of 0.03 eV/atom was required to render the enhanced motion. It is suggested that thermal fluctuation partially resolve the shear resulting from dislocation glide, such that, with an assumption that the critical shear for triggering local plastic deformation keeps constant, a larger driving force is needed at a higher temperature. Consequently the critical driving force for enhanced boundary migration increases with increasing temperature.

Fig. 4.8. GB displacement versus time at 500 K. The misorientation angle and the magnitudes of driving force are provided. Note that the transverse axis in (a-e) and (f-j) is in logarithmic and normal scale, respectively.

In the cases of the other four GBs with misorientation angles from 32.20° to 50.56°, their motion behaviors at 500 K (Figs. 4.8g-j) turned out to be quite different from what was

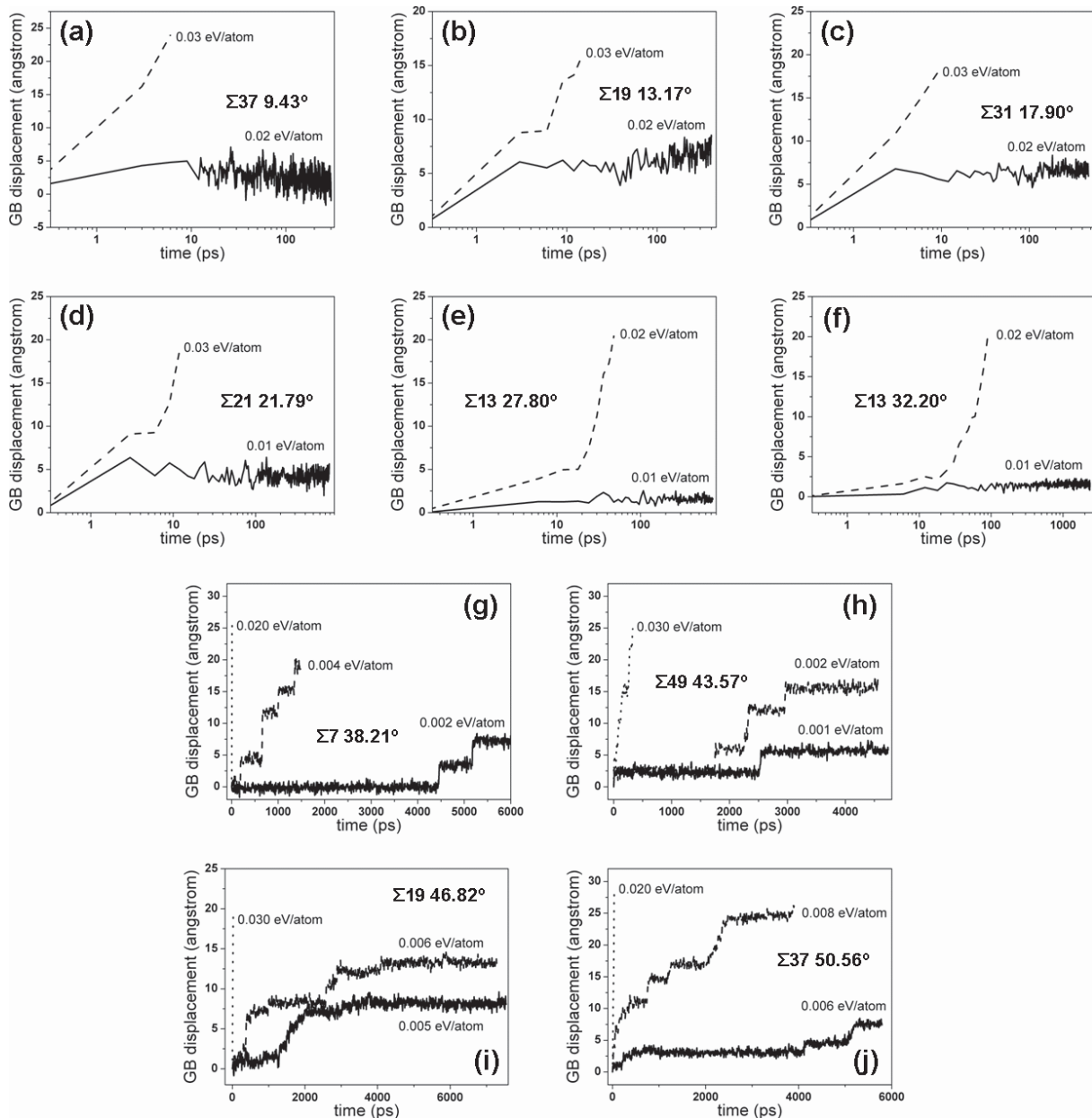observed at 10 K (Figs. 4.1g-j). During a similar simulation period, these GBs were able to displace considerably at low driving forces of several tens MPa. For example, Fig. 4.8g shows that the motion of a 38.21° GB by a driving force of 0.004 eV/atom (39 MPa) provided a 1.2 nm displacement at one nanosecond. By contrast, within the same interval, there was almost no displacement for the GB driven by a larger driving force of 0.01 eV/atom (97 MPa) at 10 K (Fig. 4.1g). The remarkable boundary motion was found to proceed in a jerky manner: a GB fluctuates for a long waiting time, and then migrates by a short step within a short time window. Furthermore, it is found that local plastic deformation never occurred with this jerky motion.

The jerky GB motion is ascribed to short-range reciprocating boundary sliding between grains, which is present in specimens with structural constraints. The unchangeable specimen shape does not allow GB sliding to develop along one single direction, rather induces back-and-forth intergranular motion. Fig. 4.3b shows the temporal evolution of grain translation for a 38.21° GB driven by a driving force of 0.004 eV/atom. The grain translation is found to oscillate frequently and be of a small magnitude up to about 0.3 Å. Compared with the evolution of GB displacement also shown in Fig. 4.3b, the translation does not correlate to the boundary migration process. During a 1.5 ns simulation, there are four GB-position jumps, whereas only the second jump is observed to correspond to a slight and temporary increase in the translation. The translation in this case therefore denotes reciprocating GB sliding inherent to GBs. Since GB sliding is thermally activated, the reciprocating extent including both frequency and amplitude is expected to depend on temperature. Functionally, the reciprocating GB sliding resolves the shear associated with GB dislocation glide, such that sustainable boundary motion without yielding local plastic deformation becomes accessible.

For the GBs that exhibit jerky motion with low driving forces, an increase in driving force to several hundred MPa caused local plastic deformation again (Fig. 4.5c). This can be explained by the limited efficiency of the reciprocating GB sliding at a certain temperature to accommodate shear. Compared with the thermally activated GB sliding, the generation rate of shear resulting from dislocation glide is proportional to boundary migration velocity, which increases with increasing driving force. There is therefore a competition between the two processes. With an increasing driving force, the reciprocating GB sliding becomes unable to sufficiently accommodate the shear, resulting in shear accumulation and subsequent local plastic deformation.

4.1.3 High-temperature behaviors

GB migration was further investigated at a high temperature 750 K (0.80 T_m). The boundary displacement-versus-time curves are plotted in Fig. 4.9. Considering the three GBs of low misorientation angles ≤ 17.90°, their motion behaviors (Figs. 4.9a-c) exhibited similar features to those observed at the two lower temperatures. By contrast, the three GBs with medium misorientation angles from 21.79° to 32.20° altered their motion behaviors to be jerky (Figs. 4.9d-f). The increase in temperature obviously reinforced the reciprocating GB sliding for the three GBs and gave rise to their jerky motion.
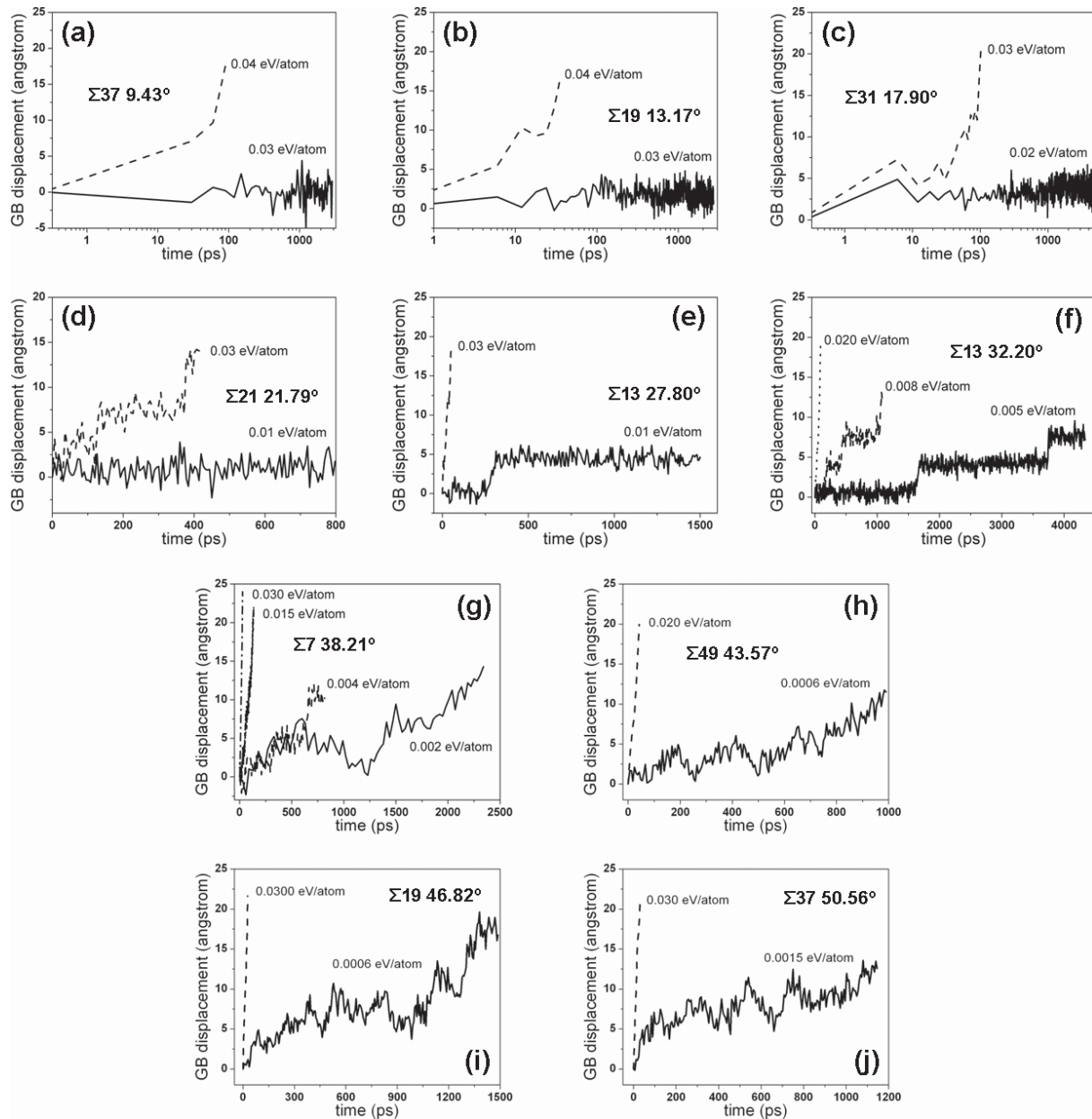
Fig. 4.9. GB displacement versus time at 750 K. The misorientation angle and the magnitudes of driving force are given. Note that the transverse axis in (a-c) and (d-j) is in logarithmic and normal scale, respectively.

Concerning the remaining four GBs of high misorientation angles, new motion behaviors were found in the cases of relatively low driving forces (< several hundred MPa). Unlike the jerky motion at 500 K, their temporal evolutions of boundary position at 750 K resembled a random walk (see Figs. 4.9g-j). The fluctuation of GB position was found not to be around any equilibrium position, such that the features of a long waiting time and rapid jump for jerky motion became absent.

The random-walk boundary motion reveals a new mechanism, which appears to be intimately related to GB structures at a high temperature. Fig. 4.10 illustrates the structures of a 38.21° <111> tilt GB at the three temperatures studied. These structures were obtained right after relaxation but before the application of driving force. We find that the GB structures at both 10 K and 500 K are thin and smooth. Each GB possesses a common plane (as indicated by a line) shared by the two neighboring grains. By comparison, the GB at 750 K turns to be thick and rough. Particularly, the GB atoms become remarkably disordered and thus there is no longer a common boundary plane. The high-temperature GB structure appears to greatly facilitate GB diffusion. An example is given for a 38.21° GB driven by a driving force of 0.004 eV/atom (37 MPa). Fig. 4.11a displays a snapshot at 750 ps, which indicates that the central GB generally didn't move, while the edge GB displaced upwards by $\sim$ 10 Å. Fig. 4.11b shows the same snapshot, but colored according to the magnitudes of atomic displacement vectors. The dark and light grey atoms indicate their displacement distances smaller and larger than the interatomic distance r_0, respectively. It is found that the atoms with displacement distance $> r_0$ concentrated in the two GBs as well as in the region swept by the edge GB. Besides, the long-distance displacement vectors were found to be isotropic. This is in contradiction to the directional atomic motions involved in the jerky boundary migration. These findings point to that GB diffusion occurred profoundly and might play an important role in the GB migration. For these diffusional atomic motions, we observed that there was a significantly enhanced diffusional flux across a GB, while the GB diffusion along a GB plane was not affected. In this regard, the GB migration mechanism could be expressed as that some atoms adjacent to a thick GB detach from the high-energy grain side, propagate along complicated trajectories in the highly disordered GB thus losing crystallinity, attach to the opposite low-energy grain side, and eventually align with the low-energy grain. Concurrently, a diffusional process along the opposite direction should happen. Overall, there is a net diffusional flux across the GB.
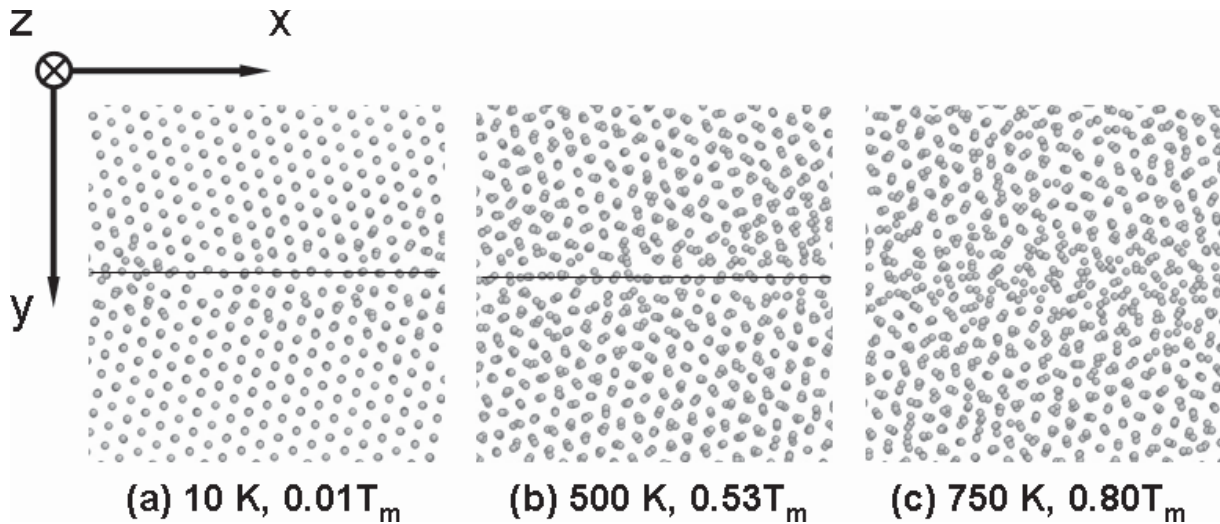
Fig. 4.10. The relaxed structures of a 38.21° GB at three temperatures. The line in (a) and (b) indicates a common boundary plane shared by two grains. All snapshots share a common coordinate system shown in the upper-left.
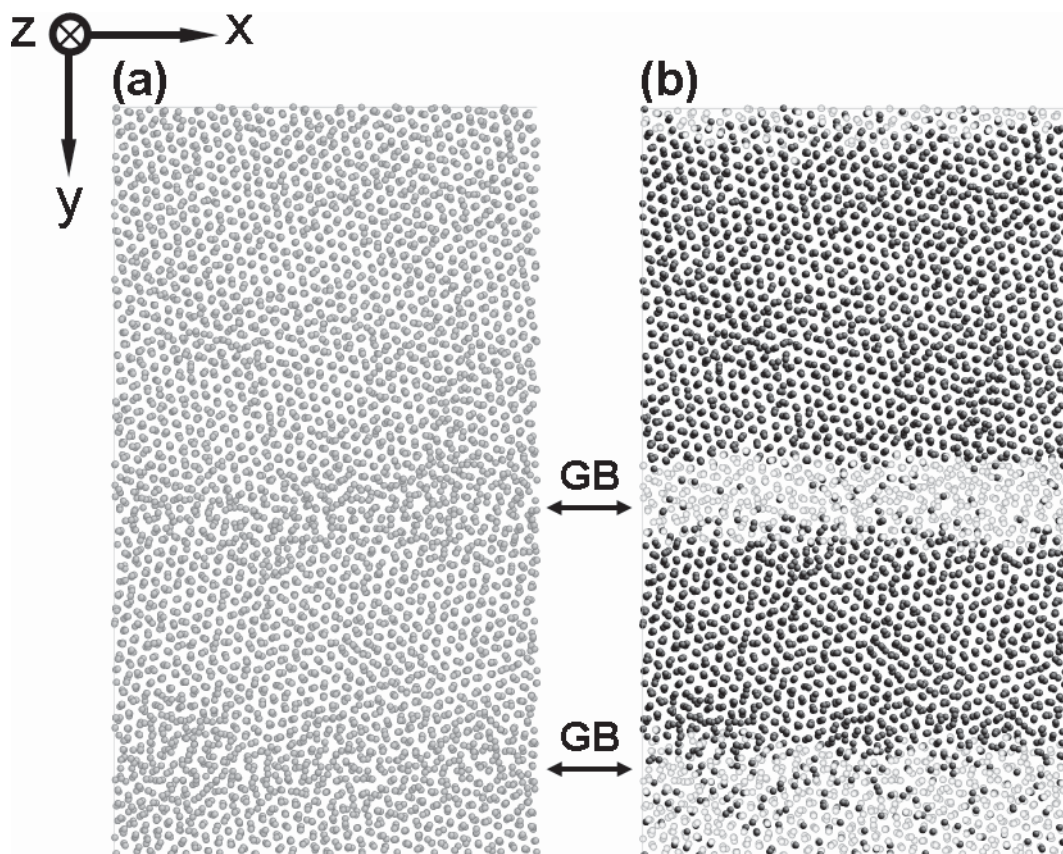
Fig. 4.11. (a) A snapshot at 0.75 ns for the migration of a 38.21° <111> tilt GB driven by a driving force of 0.004 eV/atom (~38 MPa) at 750 K. (b) represents the same snapshot as (a) but colored in accordance with the magnitude of displacement vectors. The dark and light colors denote displacement distances smaller and larger than $r_0 = 2.8$ Å, respectively. The arrows point to the GB positions. Both snapshots own a common coordinate system shown in the upper-left corner in (a).

By enlarging the driving force, it is interesting to find that the GB migration mechanism was altered from diffusional to displacive atomic motions. The CSL-shaped displacive units arising from dislocation glide were determined. The shear accompanying GB dislocation glide was resolved by the reciprocating GB sliding. When the applied driving force was sufficiently large, local plastic deformation occurred (Fig. 4.5d). To understand the mechanism change, we assume that only the atoms adjacent to a rough GB are subjected to driving forces, while there is no driving force on the atoms inside the GB (this is exactly what the application scheme of the COD-DF does, as detailed in Section 3.2.1). It is suggested that there is a competition between the entering velocities of atoms into disordered GBs and the efficiency of losing crystallinity due to diffusion. If atoms enter a rough GB at a low velocity due to a small driving force, they cannot quickly reach the opposite side. The long time for these atoms staying inside the GB causes them to be strongly affected by diffusional processes, such that the entering velocity turns to be smeared out. Consequently GB migration is controlled by GB diffusion. By comparison, if the entering velocity is high owing to a large driving force, the atoms can arrive at the opposite side quickly, as if there were no disordered GB. Thus the migration mechanism changes back to be GB dislocation glide. In function, the diffusional GB migration mechanism is therefore not capable of rendering high GB migration velocities.

4.2 Discussion

4.2.1 Migration mechanisms

Two GB migration mechanisms have been determined from our simulation results. At low (10 K) and medium (500 K) temperatures, GBs migrate through glide of GB dislocations. In order to maintain overall GB orientation, all GB dislocations need to glide cooperatively. For high-angle Σ GBs, the collective glide of GB dislocations of multiple Burgers vectors in addition induces regular distribution of CSL-shaped displacive units, which are generated by collective motion of groups of atoms of the Σ number. In this sense, the dislocation glide and the collective atomic motion are essentially equivalent, but expressed from different respects. Since the underlying atomic motions associated with dislocation glide are found to invariably

proceed along discrete crystallographic vectors, we name this mechanism displacive boundary migration (DISBM).

DISBM reconciles several mechanisms found previously in literatures. Firstly, DISBM is obviously concerted with the collective atomic motion mechanism. Secondly, the collective motion of a Σ-value amount of atoms is conceptually equivalent to the shuffling mechanism [25-28, 33]. In order to rationalize the experimental observations on the migration of near-$\Sigma 5$ GBs, Babcock and Balluffi [25] proposed a four-atom shuffling mechanism, which was subsequently supported by MD simulations [26-28, 33]. As the term 'four-atom shuffling' suggests, there are four atoms moving cooperatively along specific vectors. If one additionally takes one atom locating at a nearby coincident site into account, the atom number becomes identical to the Σ value. Finally, DISBM is compatible with the coupling mechanism [10, 35-37]. The glide of a GB dislocation naturally gives rise to grain translation and GB motion, which are perpendicular to each other. The dislocation glide therefore represents the inherent cause for coupling (note that under some conditions the shear involved in dislocation glide can be resolved by some manners other than specimen shape change, as will be discussed in Sections 4.2.2 and 4.2.3). Considering detailed atomic motions, both DISBM and the coupling show that the motion of high-angle Σ GBs is implemented by distortion and rotation of some small atom groups [10, 37].

Based on the discussion above, we suggest that DISBM represent an underlying mechanism for GB migration at low temperatures. With this mechanism, it is convenient to incorporate the motion of SGBD. This mechanism therefore readily accounts for the migration of a GB of arbitrary geometry (low-angle or high-angle; symmetric or asymmetric), since any GB at low temperatures can be geometrically described by dislocation arrangements.

The other boundary migration mechanism is merely active at high temperatures for some high-angle GBs, when a relatively low driving force is exerted. This mechanism features in diffusional atomic motions, henceforth termed diffusional boundary migration (DIFBM). With this migration mechanism, boundary migration is controlled by slow GB diffusion. Hence GB migration and GB diffusion should own comparable activation parameters, as demonstrated, to a large extent, by a large number of experiments [13-20] and one simulation [21]. Besides, since GB diffusion is expected to be active for general high-angle GBs, DIFBM could be applied to these GBs at high temperatures. It is worth mentioning that the DIFBM mechanism essentially differs from the well-known diffusion induced boundary migration

(DIGM) mechanism [93-97]. DIGM virtually denotes boundary migration by dislocation motion (compatible with DISBM however) with a driving force derived from different diffusion coefficients of components in an alloy.

4.2.2 Effect of structural constraints

Considering specific boundary motion behaviors, they are affected by many factors. In the following, we discuss some of them. In the present study, the two GBs constructed in one simulation cell, i.e. a layered polycrystalline microstructure, act as structural constraints. The structural constraints on one hand cause GB sliding to occur back-and-forth within a limited distance. On the other hand, the effect of structural constraints on boundary motion in essence lies in impeding the release of shear arising from dislocation glide through specimen shape change, and therefore inducing shear accumulation. By enlarging the applied driving force, the increasing shear could become big enough to trigger local plastic deformations, e.g. shear bands. We notice that there were no stacking faults observed, implying a high stacking fault energy (SFE) of Al described by the TB-SMA potential. For a material of low SFE, the shear could be resolved by dislocation dissociation and emission from GBs. Eventually, the boundary motion behaviors found in this study correspond to the ones in microstructures with structural constraints, but fundamentally differ from the cases without constraints as obtained in both MD simulations [10, 34, 37-40] and experiments [41-43].

It is noticeable that the structural constraints could be of various modes. In polycrystals they could be any obstacles inevitably present. In bicrystals with curved GBs driven by a capillary driving force, as performed in MD simulations [56, 60], the GB is of a changing boundary inclination angle, which gives rise to shears lying along various directions. These shears in total could compensate for each other, thus leading to zero grain translation. Moreover, structural constraints can be even active in a bicrystal of a flat GB. Zhang and coworkers [29-33, 52, 59] simulated boundary motion for a flat GB driven by the elastic energy difference in adjoining grains through biaxial strain application. They didn't observe any grain translation [29-33, 52, 59]. However, when Zhang et al. [40] altered their applied strain/stress to be uniaxial along a direction normal to both the GB normal and the boundary rotation axis, but kept the other conditions unchanged, GB migration was found to be well coupled to grain

translation. Zhang's studies evidently indicate that the loading schemes of external strain/stress can also serve as structural constraints.

It should be emphasized that the inhibition of coupled GB migration is ascribed to the structural constraints instead of the type of driving force. To validate this statement, boundary migration simulations in bicrystals without structural constraints were performed by using the same COD-DF. It was found that coupling occurred and the computed coupling factors were consistent with the predicted values.

4.2.3 Effect of temperature and misorientation angle

The effects of temperature and GB misorientation on boundary migration essentially lie in providing different GB structures, which in turn result in the diverse abilities of GB sliding, GB roughening and GB diffusion. Low-angle GB structures are commonly described as arrays of GB dislocations. The dislocation cores composed of disordered atoms are separated by elastically strained nearly-perfect regions. With increasing temperature up to the melting point, these GB structures are known to generally remain unchanged [3, 5, 53]. The condensed nearly-perfect regions suppress GB diffusion and also cause a high sliding resistance. Functionally, at any temperature, the low-angle GB structure inhibits the GB migration by DIFBM, but only allows the migration through DISBM. Given the accompanying shear cannot be accommodated by specimen shape change nor GB sliding, low-angle GBs migrate only if local plastic deformations occur as a result of large driving forces.

With an increasing misorientation angle, the distance between neighboring GB dislocation cores decreases. For high-angle GBs, dislocation cores turn to overlap completely, such that structural disorder spreads over the entire boundary planes. Moreover the degree of disorder is reported to be a function of temperature [3, 5, 7-9, 53]. At low temperatures, a high-angle GB is solid-like [3, 5], being smooth and of limited disorder as it can be described by some ordered kite-shaped structural units [1, 10, 39]. As temperature increases to a critical one T_c, a high-angle GB undergoes a reversible structural transformation to be rough and liquid-like [3, 5], thus becoming further disordered. This transformation process is referred to as GB roughening [6-9, 53]. The above description of temperature dependence of high-angle GB structures has also been observed in this study, as illustrated in Fig. 4.10.

Corresponding to the structural transformation with respect to high-angle GBs, the migration mechanism varies. For a smooth high-angle GB at temperatures lower than T_c, boundary motion proceeds by DISBM associated with the short-range reciprocating GB sliding. The sliding, prevailing due to the disappearance of any perfect crystalline region, assists the relief of the shear arising from GB dislocation glide. We therefore have the jerky boundary motion without yielding local plastic deformation. Since GB sliding is a thermally activated process, enhanced sliding at a higher temperature profoundly accelerates boundary motion such that a smaller driving force is required to achieve a certain displacement within the same period. For a rough GB at temperatures $> T_c$, it can migrate through DIFBM, as indicated by the random-walk motion. The thick and rough boundary not only favors GB diffusion but also causes migrating atoms to stay in the GB, hence losing crystallinity. Furthermore, within the regime of high-angle GBs, the ability of sliding and roughening is found to be profoundly dissimilar for different GBs. The GB migration results at 500 K in Section 4.1.2 suggest that boundary sliding is more prone to take place for GBs with larger misorientation angle. The results at 750 K in Section 4.1.3 indicate that GB roughening takes place at a lower temperature for a GB of larger misorientation angle.

It is noted that for DISBM structural constraints always cause a zero coupling factor. The reciprocating GB sliding and/or the local plastic deformations completely accommodate the shear associated with DISBM. For DIFBM, in contrast, no grain translation is required during GB motion, and thus there is virtually no coupling expected to take place even for boundary migration without structural constraints.

4.2.4 Effect of driving force magnitude

For a given GB at a certain temperature, the application of different magnitudes of driving force can give rise to fairly dissimilar boundary motion behaviors and even induce distinct boundary migration mechanisms. Generally, it is found that there are three critical driving forces $p_{c1\sim3}$ to access the diversities. p_{c1}, larger than the other two, represents the critical driving force to initiate shear bands inside grains. It has been found that a shear band always took place when a large driving force typically of several hundred MPa was applied. $p_{c2}(\Delta t)$ refers to a threshold to obtain a certain amount of boundary displacement within a designated period Δt via DISBM together with the reciprocating GB sliding. Lastly, there exists a critical

driving force p_{c3} which induces the mechanism change from DIFBM to DISBM. Considering the effective ranges of the three critical driving forces, p_{c1} is active for an arbitrary GB studied, while $p_{c2}(\Delta t)$ and p_{c3} exclusively pertain to high-angle GBs.

Each critical driving force is a function of temperature. Concerning p_{c1}, this critical driving force was found to increase as temperature increases. Suppose a given level of shear stress for shear band formation. A larger p_{c1} is required at a higher temperature, since thermal effects accommodate more shears. By contrast, p_{c2} was observed to decrease with increasing temperature. Since GB sliding is thermally activated, a lower driving force is needed at higher temperature to get certain boundary motion. Finally, because GB diffusion is thermally activated as well, the temperature effect on p_{c3} is complex. The competition between the two thermally activated processes determined the critical driving force for the mechanism change at a given temperature. Besides the thermal effect, the specific magnitudes of $p_{c1\sim3}$ ought to depend on many other factors, e.g. microstructures, GB character, materials together with interatomic potentials chosen to describe the materials. These effects remain an open question and require systematic research in the future.

4.3 Mechanism maps

There are four factors discussed in Sections 4.2.2-4.2.4 that jointly govern motion behavior for a given GB. To date, the effects of temperature and GB misorientation have been extensively considered in literatures to influence GB motion. Little attention however has been paid to the effects of microstructures and driving force magnitude. To summarize all these effects, we propose two mechanism maps for low-angle and high-angle GBs, respectively. The considered high-angle GBs are of a general character [3]. They don't need to be of Σ misorientation and can be asymmetric. Not included are some special GBs [3], e.g. coherent and incoherent twin boundaries, which exhibit contradictory motion behaviors. With the same misorientation angle, a coherent twin boundary is usually quite immobile, but an incoherent one was found to move much faster than many general high-angle GBs [69, 70]. It is emphasized that the mechanism maps are developed for an ideal system. Except for GBs, the system doesn't comprise other types of defects (vacancies, solutes, lattice dislocations etc.), which could play important roles in boundary motion under certain conditions. For example, the absence of vacancies inherently prohibits lattice diffusion, which in turn

prevents dislocation climb. In practice, the motion of low-angle GBs however could be accomplished by dislocation climb as implied by the agreement of activation enthalpy between GB migration and lattice diffusion found in shape-constrained bicrystal experiments [13-17]. In addition, the mechanism maps only apply to materials with a high SFE, and therefore dislocation dissociation at GBs are inherently not accounted for.

Fig. 4.12a illustrates the migration mechanism map for low-angle GBs. The critical driving force $p_{c1}(T)$, as discussed in Section 4.2.4, separates the map into two regimes. Below $p_{c1}(T)$, a low-angle GB is immobile (only a slight displacement after driving force application). In the cases of a driving force > $p_{c1}(T)$, a GB becomes mobile through DISBM accompanied by local plastic deformations. Fig. 4.12b displays the migration mechanism map for high-angle GBs, which shows that, apart from $p_{c1}(T)$, the other two critical driving forces $p_{c2}(T, \Delta t)$ and $p_{c3}(T)$ turn to operate. There is in addition a critical roughening temperature T_c for high-angle GBs. At a temperature lower than T_c, one cannot observe a significant amount of boundary motion within a given period of time when the applied driving force is smaller than $p_{c2}(T, t=a$ given period). For the cases of a driving force ranging from $p_{c2}(T, \Delta t)$ to $p_{c1}(T)$, a high-angle GB migrates through DISBM plus the short-distance reciprocating GB sliding. In this motion manner, it is possible to obtain sustainable boundary motion without yielding any local plastic deformation. When the driving force becomes larger than $p_{c1}(T)$, the migration manner doesn't change, but local plastic deformations have to occur. Considering the cases at temperatures > T_c, a high-angle GB migrates by DIFBM with a driving force < $p_{c3}(T)$, which doesn't yield any deformation. As the exerted driving force increases to a region from $p_{c3}(T)$ to $p_{c1}(T)$, the boundary migration mechanism changes from DIFBM to DISBM associated with the reciprocating GB sliding. If exerting a driving force larger than $p_{c1}(T)$, again local plastic deformation is required. The border of the DIFBM is shaded in Fig. 4.12b to denote a region where distinct mechanisms might coexist. It is noticeable that, since both GB sliding and GB diffusion are thermally activated, GB migration is always a thermally activated process. The motion behavior is expected to be of an unchanged activation enthalpy, if the underlying mechanism, DISBM or DIFBM, doesn't change. However, when the migration mechanism varies under some conditions, e.g. exploring boundary motion in a large temperature/driving force range, there would be a change in activation enthalpy.
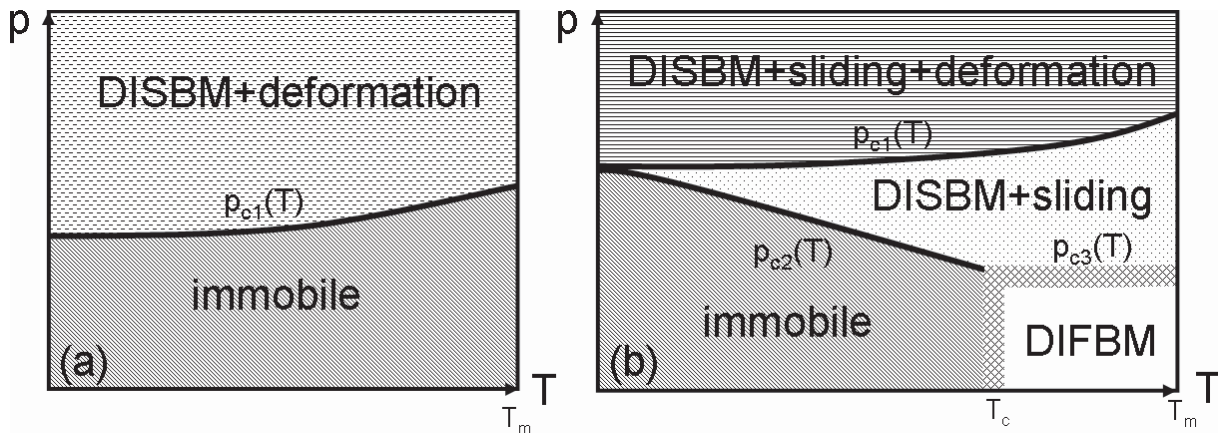
Fig. 4.12. GB migration mechanism maps for (a) low-angle and (b) high-angle GBs with structural constraints.

Fig. 4.12, derived from the present simulation, describes the boundary migration manner qualitatively. Nevertheless, the validity of the two proposed mechanism maps is supported based on that many previous findings, which are frequently in contradiction of one another, can be well rationalized. A large body of experimental observations, consisting of boundary motion during recrystallization and grain growth in commercial polycrystalline alloys and in bicrystals with structural constraints, was always obtained with a relatively low driving force (e.g. ~10 MPa for heavily cold worked metals) at high temperatures. Based on the mechanism maps, it is therefore expected that GB migration involved proceeds by DIFBM. The fact that DIFBM is only in function for high-angle GBs likely accounts for the widely reported finding that high-angle GBs move much faster than low-angle GBs. The DIFBM mechanism is further implied by the agreement of activation enthalpy between GB migration and GB diffusion in various processes and materials, e.g. recrystallization of a high-Mn steel [18], bicrystal experiments in high-purity metals [12-17] and even grain growth simulation [21].

Recently, grain growth was observed at low homologous temperatures in fine-grained and nanocrystalline metals [44-48]. The authors ascribed the involved boundary motion to the coupling mechanism, but meanwhile measured smaller coupling factors than the theoretically predicted ones by Suzuki et al. [37] and Cahn et al. [10]. Caillard et al. [36] proposed a model to rationalize these phenomena as the motion of an arbitrary GB (not Σ GBs) through disconnection (SGBD) glide together with local collective motion of groups of atoms. It was thought that the former and latter yielded a predicted and a zero coupling factor, respectively. The two contributions finally produced a medium coupling factor. Nevertheless, as discussed in Section 4.2.1, the glide of SGBD and the collective atomic motion essentially are unified in

DISBM. This mechanism gives a predicted and a zero coupling factor in microstructures without and with structural constraints, respectively.

To rationalize the medium coupling factor, a new consideration is suggested. We firstly note that, for materials of small grain size, a large internal stress, e.g. estimated value = 200 MPa in [47], can occur because of the lack of dislocation-mediated plasticity. Hence, the large stress renders boundary motion by DISBM. Secondly, it is common to find more excess volume, e.g. pores, in nanocrystals than in polycrystals. The exact magnitude of excess volume is highly dependent on the synthesis and processing history of given materials, as reviewed by Meyers et al. [98]. The excess volume allows shape change of crystallites. In this sense, the microstructure can be thought of as a combination of two partitions: one without constraints and the other with constraints. For the former and latter, a predicted and a zero coupling factor occur, respectively. On average, medium coupling factors are readily understood. It is therefore concluded that the coupling is always induced by stress, while the extent of grain translation (strain) observed in practice is expected to increase with increasing excess volume.

Due to the inherent timescale limitation, most MD simulations [9, 10, 26-28, 34, 37, 39, 40, 54, 56, 60, 69, 70] utilized very large driving forces typically of several hundred MPa, so that one can observe boundary motion. According to our mechanism maps, these large driving forces always cause boundary motion by DISBM. Given the boundary motion through DIFBM in high-temperature experiments, the fundamental discrepancy of migration mechanism reasonably accounts for the different activation enthalpies measured in experiments and simulations [27, 52, 56, 60].

Chapter 5

Mobility evaluation

In this chapter, we focus on mobility evaluation for the set of symmetric <111> tilt GBs as discussed in Chapter 4 at a high temperature 750 K ($0.8T_m$). Among these boundaries, the $\Sigma 7$ 38.21° GB is of particular importance due to its relevancy to abnormal grain growth. This GB has been studied in detail [11, 19, 60, 64, 67, 69, 99], thereby allowing comparisons with previous computational and experimental studies. Before the mobility evaluation, the relationship between GB migration velocity and driving force (typically much larger than the ones employed in bicrystal experiments) is firstly investigated. A nonlinear relationship instead of proportionality occurs in MD simulations. By evaluating GB mobility nonlinearly, the computed mobilities show reasonable misorientation dependence. In particular, by comparing the mobilities of the $\Sigma 7$ GB obtained through different methods, the performance of our driving force application approach for mobility prediction is demonstrated.

5.1 Nonlinear relationship between migration velocity and driving force

With the new approach of COD-DF application as discussed in Section 3.2, the selected tilt GBs were investigated with respect to the relation between GB velocity v and driving force p. Owing to the intrinsic limitation of MD timescale, the temperature studied has to be high, and

the driving force has to be much larger than the experimental ones, such that one is able to observe GB motion in the available period of time. In this study, the temperature was set to 750 K. Our driving force ranged from 0.001 to 0.007 eV/atom (about 10~70 MPa). Within this range together with a simulation time window of several ns, according to the migration behaviours found in Section 4.1.3, it is known that only the five high-angle GBs with $\theta \geq 32.20°$ are mobile. Furthermore, based on the migration mechanisms discussed in Section 4.2, the $\Sigma13$ 32.20° GB migrates through DISBM plus the short-range reciprocating boundary sliding; the other four GBs through DIFBM.

Fig. 5.1 plots all the simulated migration velocities as a function of the applied driving force. Irrespective of the difference in migration mechanisms, a nonlinear relation between v and p was always revealed for all the mobile high-angle GBs, unlike in many other MD simulations which observed or assumed a proportional relation [27, 69, 100]. We further find that the nonlinear relation can be fully attributed to the large driving forces used in MD, as expected by rate theory, which predicts

$$v = w\omega e^{\frac{S}{k_B}} e^{-\frac{H}{k_B T}} (e^{\frac{pV}{k_B T}} - 1) \qquad\qquad \textbf{(5.1)}$$

where the parameters have been explained already in Section 2.2. For MD simulations, the applied driving force p is so large that its product with V becomes comparable to $k_B T$. Hence nonlinearity between v and p can be expected to occur. In Fig. 5.1, the simulated v-p data is plotted together with Eq. (5.1) fitted to these data. Obviously the nonlinearity is described by rate theory very well in all cases. In MD simulations in literature, this has not been considered or mentioned so far.
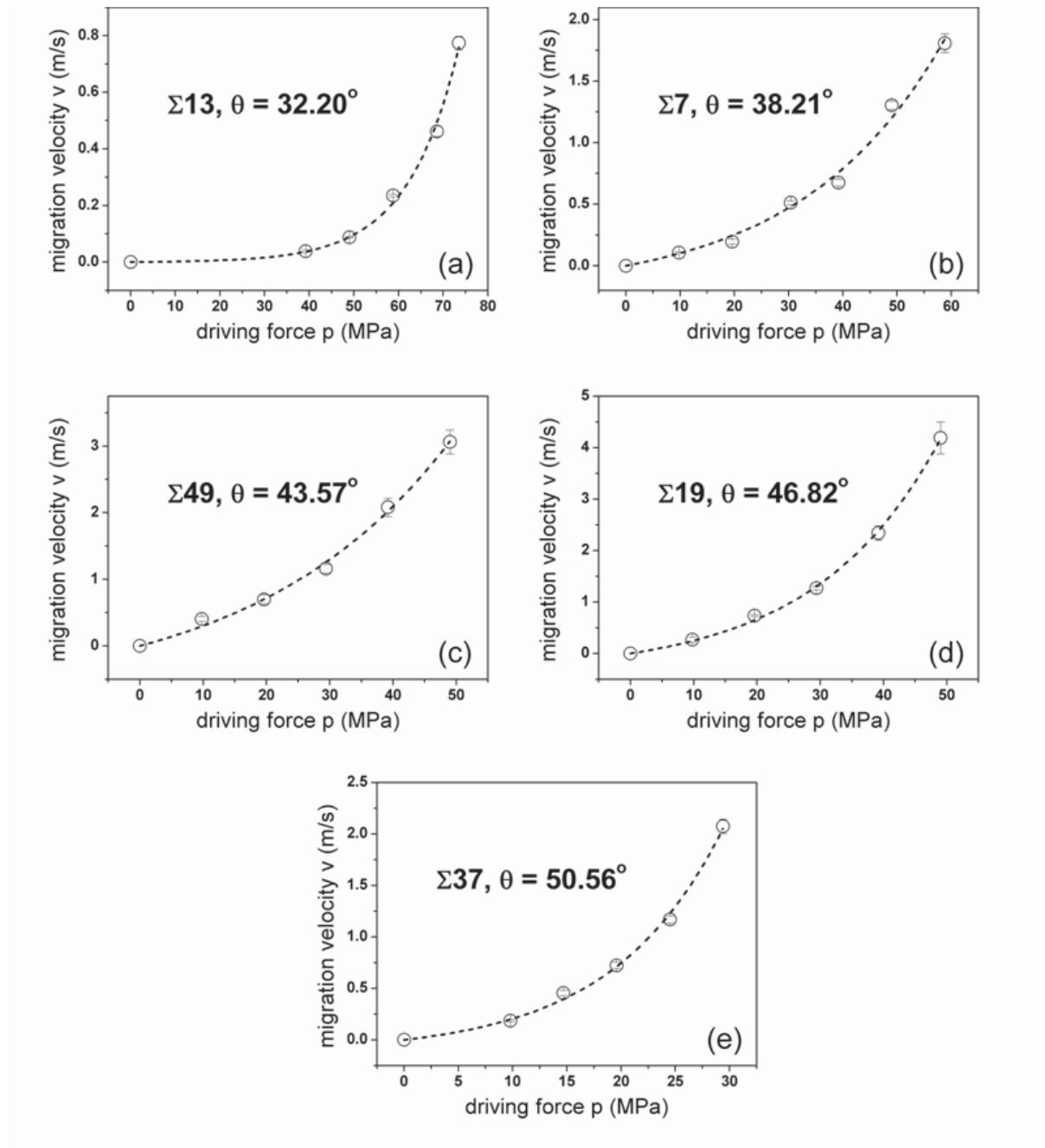
Fig. 5.1. Simulated GB migration velocity versus driving force. The data are fitted by Eq. (5.1). The error bars are derived in the way as indicated in Sec. 3.2.1.

5.2 Misorientation dependence of grain boundary mobility

The conventional definition of mobility m is based on the proportionality between v and p. For a nonlinear relationship, as found in section 5.1.1, a different definition of m is needed. In Ref. [52], it was suggested that the mobility should be uniquely defined in the low driving force limit:

$$m = (\frac{\partial v}{\partial p})_{p \to 0} \qquad\qquad\qquad \textbf{(5.2)}$$

With this equation, the mobilities of the GBs studied in this work were calculated from their fits of v-p data to Eq. (5.1). The yielded mobilities m for the studied <111> GBs at 750 K and the corresponding volumes V are listed in Table 5.1; m is also plotted as a function of misorientation angle in Fig. 5.2.

Fig. 5.2 demonstrates that the computed mobility generally increases with rising misorientation angle. Within the mobility resolution of about 10^{-10} $m^4J^{-1}s^{-1}$ defined by the finite simulation time (see Σ13 32.20° in Table 5.1), the first 5 GBs with θ up to 27.8° were immobile. The further increment of θ led to a significant increase in boundary mobility. The maximum mobility was found be to occur around 40°. Considering low-angle GBs and high-angle GBs, the former obviously move much more slowly than the latter. All these behaviours are consistent with experimental observations, but contradicts the finding in [70] with the original COD-DF.

Table 5.1. The ten symmetric <111> tilt GBs in Al[*]

θ (°)	Σ	GB plane	m (10^{-8} m^{4}J^{-1}s^{-1})	V (Ω)
9.43	low-angle	(10 11 1)	$< 1.0 \times 10^{-2}$	—
13.17	low-angle	(7 8 1)	$< 1.0 \times 10^{-2}$	—
17.9	31	(5 6 1)	$< 1.0 \times 10^{-2}$	—
21.79	21	(4 5 1)	$< 1.0 \times 10^{-2}$	—
27.8	13	(3 4 1)	$< 1.0 \times 10^{-2}$	—
32.2	13	(5 7 2)	$(1.1 \pm 0.43) \times 10^{-2}$	54 ± 3.5
38.21	7	(2 3 1)	$(8.4 \pm 2.0) \times 10^{-1}$	24 ± 2.6
43.57	49	(5 8 3)	2.6 ± 0.53	20 ± 2.3
46.82	19	(3 5 2)	1.9 ± 0.19	32 ± 1.3
50.56	37	(4 7 3)	1.2 ± 0.19	61 ± 3.4

[*] θ, misorientation angle; Σ, the reciprocal coincidence site density; m, simulated grain boundary mobility; V, average volume involved in boundary migration processes in units of the atomic volume $\Omega = 16.6$ Å^3.
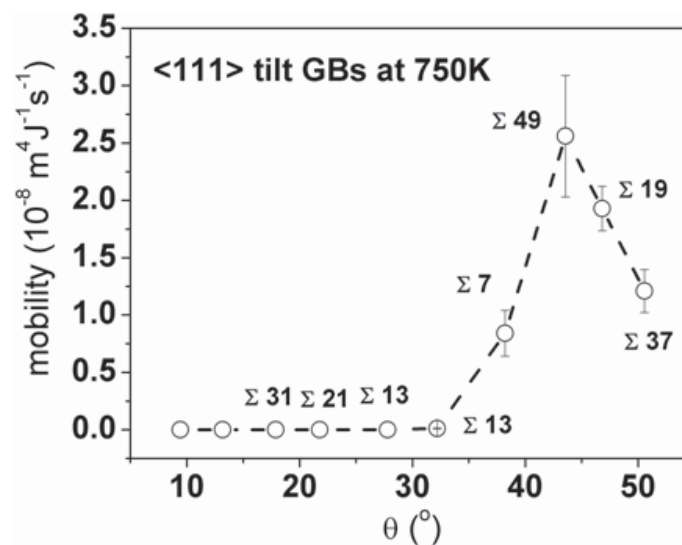

Fig. 5.2. Simulated misorientation dependence of GB mobility for symmetric <111> tilt GBs at 750 K.

5.3 Discussion

The nonlinear relationship between GB velocity and driving force has also been mentioned explicitly in MD simulations by other groups using two different driving forces [52, 65]. However, a convincing explanation has not been given. In the present study the nonlinear relationship is fully rationalized by reaction rate theory, as evidenced by Fig. 5.1. In Refs. [52] and [65], an elastic driving force and a driving force derived from a dislocation density difference in neighboring grains (resembling real driving forces in metals during recrystallization), respectively, were employed. The natures of these two driving forces clearly differ from the present artificial one, but in all three cases a non-linear relation is found. We therefore suggest that the nature of driving force is not the principle cause for the nonlinearity. Instead, the main cause is described by rate theory.

Owing to the high density of coincidence sites of the Σ GBs investigated here, it is suggested that these GBs might be of high mobilities. In this work, the Σ values associated with the studied GBs, given in Fig. 5.2, however indicate that there is no correlation between the Σ values and the magnitudes of mobility. For instance, the $\Sigma49$ GB possesses a larger mobility than its two adjacent neighbors, the $\Sigma7$ and $\Sigma19$ GBs.

As mentioned above, the $\Sigma7$ GB ($38.21°$) has been studied extensively in literature. To get our result into perspective, Table 5.2 lists the mobilities of this boundary obtained in previous experiments as well as MD simulations under similar conditions. The computed mobility in the present work represents by far the smallest value of the listed MD results (rows 1-6) found for essentially the same temperature. The difference is 1-3 orders of magnitude, varying with the MD potential and the driving force employed.

Particularly, we find that our new approach results in a smaller mobility than the one obtained with the original COD-DF application (row 2). A direct comparison between the two mobilities reflects a factor of about 7. If the temperature difference is taken into account, the factor reduces to 3.5 by supposing $H_{GBM} = 0.7$ eV [11]. The drop in mobility is likely due to the improvements to the COD-DF application together with the nonlinear evaluation of mobility. The latter will always tend to yield lower values (Eq. (5.2) instead of $m = v/p$); the effects of the COD-DF are much more difficult to understand as outlined in section 3.2.1.

Meanwhile, our mobility is found to approach the maximum experimental results (rows 7 and 8) obtained in ultra-high purity Al bicrystals.

We also note that the two simulation results using a random walk method [67] (rows 3 and 4) were obtained with exactly zero driving force. This is equivalent to our simulated mobility extrapolated with Eq. (5.2). Nevertheless, the mobilities resulting from the random walk method are found to be much larger than ours. The cause of this difference is probably linked to the different MD potentials used.

Table 5.2. Mobilities of 38.21° <111> boundary in Al at homologous temperatures from 0.8 to 0.9T$_m$. The rows 1-6 concern molecular dynamics simulations and 7-8 refer to bicrystal experiments; rows 2-8 are adopted from [67]. Also given are the corresponding potentials for simulated results and the type and magnitude of driving force for all results.

	GB	Potential	T (K)	Driving force p (Pa)	Mobility (m^{4}J^{-1}s^{-1})
1	Flat	TB-SMA	750 (0.8T$_m$)	COD-DF, p ~ 10^6	$(8.4\pm2.0)\times10^{-9}$ this work
2	Flat	EAM	800 (0.86T$_m$)	COD-DF, p ~ 10^8	6.0×10^{-8} [69]
3	Flat	EAM	750 (0.8T$_m$)	Random walk, p ~ 0	4.4×10^{-7} [67]
4	Flat	LJ	840 (0.9T$_m$)	Random walk, p ~ 0	7.7×10^{-8} [67]
5	Flat	LJ	840 (0.9T$_m$)	Deformation, p ~ 10^7	1.3×10^{-8} [64]
6	Curved	EAM	750 (0.8T$_m$)	Curvature, p ~ 10^7	1.0×10^{-6} [60]*
7	Curved	(exp.)	758 (0.81T$_m$)	Curvature, p ~ 10^3	5.0×10^{-9} [11]*
8	Curved	(exp.)	758 (0.81T$_m$)	Curvature, p ~ 10^2	3.5×10^{-9} [11, 73]*

* Curved GBs with a constant overall misorientation, comprising a range of inclination. Consequently only the inclination-averaged reduced mobility $m^* = m\Gamma$ is obtainable. To get the absolute mobility m, the GB stiffness Γ is assumed to be 0.5 J/m^2.

According to the fits of v-p data to Eq. (5.1), shown in Fig. 5.1, the two additional terms V and $w\omega e^{\frac{S}{k_B}} e^{-\frac{H}{k_B T}}$ can be evaluated, besides the mobility. The obtained V values for the mobile GBs are given in Table 5.1. The large V magnitudes, ranging from 20 to 61 atomic volumes in Al, indicate that the migration of the GB was indeed implemented by large groups of atoms. This is consistent with the DISBM mechanism for the migration of the Σ13 32.20° GB. For the DIFBM mechanism associated with the other four GBs, the large measured V suggests that, before and after the diffusional atomic motions through a rough GB, atom groups possibly need to decompose from the shrinking grain and reconstruct to the growing grain, respectively. Besides, for the 38.21° Σ7 boundary, V is determined to be 24 atomic volumes. This value is very close to the size of the equilibrium unit structure of the given boundary,

found by Bachurin et al. [101], in which the unit structure contains 23 atomic volumes, and is positioned periodically along the boundary plane. Future investigations will reveal whether this agreement is coincidence or a hint to the effective migration mechanism.

In order to further assess whether or not our simulation results are reasonable, we examine m_0 as defined by Eq. (2.7). Knowing k_BT, $V = 24\Omega$, the activation entropy $S = 11.25$ $JK^{-1}mol^{-1}$ equal to the fusion entropy in Al [102], and $w = \sim 5$ Å for a rough boundary (Fig. 4.11), and assuming an attack frequency of $\omega = 10^{13}$ s^{-1} close to the Debye frequency, we find $m_0 = 7.5\times10^{-4}$ $m^4J^{-1}s^{-1}$. This is in very reasonable agreement with the preexponential factor m_0 of 1×10^{-4} $m^4J^{-1}s^{-1}$, which has been experimentally derived for the 38.21° $\Sigma7$ boundary in ultra-high purity Al bicrystals with an impurity level of a few ppm [11]. Furthermore, using the simulated mobility m and the simulated value of m_0, the activation enthalpy of migration is found to be $H_{GBM} = 0.74$ eV. This obtained value represents, to our knowledge, the largest one in all MD simulations for various GBs in any material, and in fact closely approaches the minimum experimental result of 0.7 eV obtained in Al bicrystals [11], indicating that both these experiments and our simulations already reflect the intrinsic boundary motion behaviours. Of course, the conventional way to obtain the two activation parameters m_0 and H is to use boundary mobilities at different high temperatures with the same migration mechanism. This requires a systematic investigation which is beyond the scope of this study. However, the estimations given here appear to be physically reasonable in all respects.

Chapter 6

Summary

In summary, GB migration was simulated by MD for a set of <111> tilt GBs in Al. To drive GB motion, an artificial driving force, namely COD-DF, was utilized. We firstly analyzed the shortcoming of the original method for COD-DF application in previous studies [69, 70]. A single order parameter cannot clearly discriminate the structures of the GBs and the grain insides, resulting in the driving force on boundary atoms to be incorrect. To resolve this shortcoming, a new approach using two order parameters and three discrete states of added energy has been proposed. An effective force on the individual GB atoms based on these energies has been suggested and verified by the work of driving force associated with the motion of grain boundaries.

With the new approach, GB migration was extensively investigated in a wide temperature range ($0.01T_m \leq T \leq 0.80T_m$) with different magnitudes of driving force. Through examining the atomic motions during GB migration, there are two mechanisms determined. Under different conditions, a GB migrates through either displacive or diffusional atomic motions. The former and latter have been termed DISBM and DIFBM, respectively.

The fundamental reason for DISBM is boundary motion by GB dislocation glide. For high-angle Σ GBs, the collective glide of GB dislocations of multiple Burgers vectors in

superposition induces regular distribution of CSL-shaped displacive units, which are accomplished by collective motion of groups of atoms of the Σ number. In this sense, the dislocation glide and the collective atomic motion are essentially equivalent, but expressed from a different point of view. The DISBM mechanism is compatible with some mechanisms found in previous studies. These mechanisms consist of the collective atomic motion [25-32], the shuffling [25-27, 33] and the coupling between GB migration and grain translation [10, 34-49]. The DISBM mechanism serves as a generalized model for these three. This mechanism not only sheds light on the inherent reason for the occurrence of the coupling but also clearly demonstrates the intimate connection between the GB dislocation glide and the collective motion of atom groups. Furthermore, the DISBM mechanism is convenient to be extended to include the motion of secondary GB dislocation for asymmetric GBs, and therefore is capable of describing the motion of a GB of arbitrary geometry.

By contrast, the DIFBM mechanism is shown to be controlled by slow GB diffusion. This is consistent with the experimentally observed agreement of activation enthalpy between GB migration and GB diffusion, which is widely reported in literatures. Akin to DISBM, DIFBM should also be insensitive to GB geometry and thus could be applied to general high-angle GBs.

Under certain conditions, local plastic deformations (shear bands and distortion of GB dislocation cores) and GB sliding (in a reciprocating mode) are found to occur during GB migration. It is these processes together with the two boundary migration mechanisms that eventually determine the motion behavior of a given GB.

The selection of the two boundary migration mechanisms and the extent of the two processes, i.e. local plastic deformation and GB sliding, are observed to be affected by many factors consisting of structural constraints, temperature, boundary misorientation angle and magnitude of driving force. In particular, the effect of structural constraints on GB migration is, to our best knowledge, for the first time systematically elucidated. The structural constraints cause local plastic deformations (indicating a mechanism of shear band formation) and GB sliding in a reciprocating mode, both of which in turn thoroughly accommodate the shear associated with DISBM and suppress grain translation.

We notice that in practical materials there is excess volume (e.g. porosities), which permits local ideal coupling between GB migration and grain translation. The shear accommodation and the effect of excess volume therefore rationalizes the smaller (but non-zero) coupling factors, as measured in low-temperature grain growth experiments [44-48], than theoretically predicted values [10, 37]. It is further concluded that the coupling is induced by stress, while the extent of grain translation or strain observed in practice is expected to increase with increasing excess volume. It is worth mentioning that GB migration through DIFBM at high temperatures doesn't yield shear. Thus there is fundamentally no coupling.

The two factors of temperature and boundary misorientation angle together determine GB structures. Low-angle GB structures comprise nearly-perfect crystalline regions at any temperature. These regions inhibit GB sliding and GB diffusion. For a microstructure with structural constraints, low-angle GBs therefore can only migrate with a sufficiently large driving force which triggers local plastic deformation to accommodate the shear associated with GB dislocation glide. The structures of high-angle GBs are of a limited degree of disorder at low temperatures and become thoroughly disordered as a bulk liquid at high temperatures. These structures always favor GB sliding. The high-temperature structure in addition causes GB migration by DIFBM. With increasing temperature, there is therefore a migration mechanism change from DISBM to DIFBM for high-angle GBs.

The effect of magnitudes of driving force on boundary motion is for the first time reported. The driving force value is closely related to the formation of local plastic deformations. Furthermore, interestingly, as the driving force applied for high-angle GBs increases, the migration mechanisms is found to change from DIFBM to DISBM. Considering the large magnitudes of driving force applied in many previous MD studies [9, 27-33, 52, 56, 60, 69, 70], our finding points to that the boundary motion investigated in these studies very likely proceeded by DISBM, differing from the GB migration via DIFBM in experiments on recrystallization and grain growth.

There are two competitions between two pairs of processes observed in this study. The first competition happens between the generation rate of geometrically necessary shear as a function of migration rate and the efficiency of shear accommodation by the reciprocating GB sliding as a function of temperature. Once the shear cannot be totally resolved by the reciprocating GB sliding, shear stress accumulates to a critical value for local plastic

deformations. The other competition is expected to be valid for high-angle GBs at high temperatures. The competition exists between the entering velocity of atoms into a highly disordered GB and the efficiency of losing crystallinity of these atoms by GB diffusion. This competition accounts for the mechanism change as the applied driving force varies.

Based on our findings above, two qualitative mechanism maps for low-angle and high-angle GBs, respectively, are proposed. The two maps are verified by various previous observations of GB migration in both experiments and simulations. Particularly, these previous observations were often in contradiction of one another. But they are reconciled within our mechanism maps.

After knowing the migration mechanisms, the mobilities for the <111> tilt GBs at the highest temperature $0.80T_m$ have been evaluated. To do that, the relation between GB velocity and driving force was checked and demonstrated to be nonlinear, irrespective of the underlying mechanism DISBM or DIFBM. The nonlinear relation was further found to be in full accordance with rate theory for large driving forces. Using this theory for evaluation, the GB mobilities for realistically low driving forces through a nonlinear evaluation method have been derived. The computed mobilities indicate that high-angle GBs are much more mobile than low-angle GBs; the maximum occurs around 40°. All these findings are consistent with experimental observations in recrystallization and grain growth.

At the same time, the evaluation method yields an effective volume that is involved in the underlying migration mechanism. The computed volume is found to be in a range of 20 to 61 atomic volumes. This large volume provides additional evidence that GB migration through DISBM is indeed enabled via correlated motion of atom groups. Also, it suggests that, even for the migration through DIFBM, before and after the diffusional atomic motions across a rough GB, atom groups need to decompose from the shrinking grain and reconstruct to the growing grain, respectively. In addition, since the effective volumes can be large, all mobility evaluations of driven GB simulations must be evaluated by nonlinear rate theory, using at the very least two magnitudes of driving force.

Moreover, the 38.21° Σ7 GB has been studied in more detail through comparisons with literature. Compared with other MD simulated results for this GB, the presently simulated mobility has by far the smallest value. This value for the first time approaches the maximum

experimental results reported in literatures. For the same GB, its activation enthalpy is assessed to be 0.74 eV. This magnitude represents the largest value found in all MD simulations and approaches the minimum experimental value of 0.7 eV measured in high purity Al bicrystals [11]. Since all our simulations concerns pure metal, the agreements of the mobility and the activation enthalpy between simulations and experiments in addition imply that the effect of impurity drag on boundary motion might be drastically overestimated for ultra-high-purity metals.

Altogether, our new approach of COD-DF application has been demonstrated to describe GB migration in a physically reasonable manner. The present study by MD simulations greatly gives insight into GB migration mechanisms. Also it shows the potential to predict experimentally comparable mobility values, as well as activation parameters.

7. Zusammenfassung

Korngrenzenmigration wurde mit Hilfe der Molekulardynamik für einen Satz von <111>-orientierten Korngrenzen in Al simuliert. Um die Korngrenzen zu bewegen, wurde eine künstliche Antriebskraft, namens COD-DF, eingesetzt. Zunächst wurden in ersten Untersuchungen die Nachteile der COD-DF Methode in ursprünglicher Version analysiert. Dabei wurde festgestellt, dass ein einzelner Ordnungsparameter nicht in der Lage ist, die Struktur der Korngrenzen eindeutig vom Inneren beider Körner zu unterscheiden. Das führt dazu, dass die Antriebskraft für die Atome an den Korngrenzen nicht korrekt ist. Um diesen Fehler zu korrigieren, wurde ein neuer Ansatz vorgeschlagen und verwendet, in dem zwei Ordnungsparameter und drei diskrete Energiezustände verwendet werden. Auf Basis dieser Energien wurde eine effektive Kraft auf einzelne Atome an den Korngrenzenatomen formuliert und über die mit der Bewegung der Korngrenzen zusammenhängende Arbeit der Antriebskraft verifiziert.

Mit diesem neuen Ansatz wurde die Korngrenzenmigration in einem weiten Temperaturbereich mit unterschiedlich großen Antriebskräften ausführlich untersucht. Durch Untersuchung der atomaren Bewegungen während der Korngrenzenmigration sind zwei Mechanismen definiert worden. Abhängig von bestimmten Bedingungen kann eine Korngrenze entweder durch einen verschiebenden oder einen diffusionsbasierten Mechanismus migrieren. Diese zwei Mechanismen werden als DISBM (displacive boundary motion) bzw. DIFBM (diffusive boundary motion) bezeichnet.

Die grundlegende Ursache für DISBM ist die Korngrenzenbewegung durch das Gleiten von Korngrenzenversetzungen. Für großwinklige Σ-Korngrenzen bewirkt das kollektive Gleiten von Korngrenzenversetzungen mit verschiedenen Burgersvektoren, dass Atome sich gruppenweise in CSL-förmigen Einheiten, sogenannten "Displacive Units" umordnen, die aus einer Anzahl von Σ Atomen bestehen und regelmäßig angeordnet sind. In diesem Sinne sind das Gleiten der Versetzungen und die gruppierten atomaren Bewegungen im Wesentlichen äquivalent, aber unter einem anderen Gesichtspunkt ausgedrückt. Der DISBM-Mechanismus ist kompatibel mit diversen anderen Mechanismen aus früheren Untersuchungen. Diese Mechanismen bestehen aus kollektiven atomaren Bewegungen, sowie der Verschachtelung und Kopplung zwischen der Korngrenzenmigration und der Korntranslation. Der DISBM-Mechanismus dient als ein verallgemeinertes Model. Er gibt nicht nur Aufschluss über die inhärente Ursache der Existenz der Kopplung, sondern demonstriert auch den engen Zusammenhang zwischen dem Gleiten der Korngrenzen und der kollektiven Bewegung der Atomgruppen. Der DISBM-Mechanismus erlaubt auch eine einfache Erweiterung auf die Bewegung sekundärer Korngrenzenversetzungen in asymmetrischen Korngrenzen, und kann daher die Bewegung von Korngrenzen beliebiger Geometrie beschreiben.

Es wurde gezeigt, dass der DIFBM-Mechanismus im Gegensatz zu DISBM durch die langsame Korngrenzendiffusion bestimmt wird. Dies ist durch die in der Literatur experimentell beobachtete Übereinstimmung der Aktivierungsenthalpie von Korngrenzenmigration und Korngrenzendiffusion untermauert.

Unter bestimmten Bedingungen treten lokale plastische Verformungen (Scherbänder bzw. Verzerrung von Korngrenzenversetzungskernen) und Korngrenzengleiten während der Korngrenzenmigration auf. Zusammen mit den zwei Mechanismen der Korngrenzenmigration bestimmen diese Prozesse letztendlich das Bewegungsverhalten einer bestimmten Korngrenze.

Es wurde beobachtet, dass die Auswahl des aktiven Migrationsmechanismus (lokale plastische Verformung oder Korngrenzengleiten) bzw. das Ausmaß derer Aktivitäten von vielen Faktoren beeinflusst werden, wie zum Beispiel strukturelle Bedingungen, Temperatur, Fehlorientierungswinkel und Größe der Antriebskraft. Insbesondere ist die Wirkung der strukturellen Bedingungen auf die Korngrenzenmigration, nach unserem besten Wissen, erstmals systematisch geklärt worden. Die strukturellen Bedingungen führen zu lokalen plastischen Verformungen (die auf einen Mechanismus der Scherbandbildung hinweisen) und

ruckartigem Korngrenzengleiten, die beide vollständig die mit DISBM verbundene Scherung ausgleichen und Korntranslation unterdrücken.

Es ist anzumerken, dass es in echten Materialien Überschussvolumen gibt, das eine lokale ideale Kopplung zwischen Korngrenzenbewegung und Korntranslation ermöglicht. Die Scherungsausgleich und die Wirkung von überschüssigem Volumen erklärt daher die im Vergleich zur theoretischen Vorhersage kleineren (aber nicht verschwindenden) Kopplungsfaktoren, wie sie in Kornwachstumsexperimenten bei niedrigen Temperaturen gemessen wurden. Es wird weiter festgestellt, dass die Kopplung durch Spannung induziert wird, während das Ausmaß der Korntranslation oder die in der Praxis beobachtete Dehnung mit zunehmendem Überschussvolumen steigt. Es ist erwähnenswert, dass die Korngrenzenmigration durch DIFBM bei hohen Temperaturen keine Scherung ergibt. Deshalb gibt es dabei grundsätzlich keine Kopplung.

Die zwei Faktoren, also die Temperatur und der Fehlorientierungswinkel an der Korngrenze, bestimmen gemeinsam die Korngrenzenstruktur. Die Strukturen der Kleinwinkelkorngrenzen bestehen bei jeder Temperatur aus nahezu perfekt kristallinen Bereichen. Diese Bereiche verhindern ein Korngrenzengleiten und die Korngrenzendiffusion. Für eine Mikrostruktur mit strukturell verhinderter Korntranslation können daher die Kleinwinkelkorngrenzen nur migrieren, wenn eine ausreichend großen Antriebskraft vorliegt, die lokale plastische Verformungen zur Aufnahme der mit dem Korngrenzengleiten verbundenen Scherung ermöglicht. Die Strukturen der Großwinkelkorngrenzen haben bei niedrigen Temperaturen einen begrenzten Grad, und bei hohen Temperaturen einen erheblichen Grad an Unordnung ähnlich einer Flüssigkeit. Diese Strukturen begünstigen immer das Gleiten der Korngrenzen. Die Hochtemperaturstruktur ermöglicht zusätzlich eine Korngrenzenmigration durch DIFBM. Mit steigender Temperatur ergibt sich daher für Großwinkelkorngrenzen ein Wechsel des Migrationsmechanismus von DISBM zu DIFBM.

Die Einfluss der Größe der Antriebskraft auf die Korngrenzenbewegung wurde erstmals systematisch untersucht. Die Stärke der Antriebskraft hat einen großen Einfluss auf die Bildung der lokalen plastischen Verformungen. Darüber hinaus wurde interessanterweise festgestellt, der Migrationsmechanismen bei Großwinkelkorngrenzen von DIFBM zu DISBM wechselt, wenn die Antriebskraft über ein gewisses Maß zunimmt. Unter Berücksichtigung der in früheren Untersuchungen verwendeten großen Antriebskraft, weisen unsere Ergebnisse darauf hin, dass die Korngrenzenbewegung in diesen Untersuchungen sehr wahrscheinlich

aus DISBM entsteht, was sich von der Korngrenzenmigration durch DIFBM in Experimenten zu Rekristallisation und Kornwachstum unterscheidet.

Es sind zwei konkurrierende Effekte zwischen zwei Paaren von Prozessen in dieser Untersuchung zu beobachten. Die erste Konkurrenz tritt zwischen der Erzeugungsrate der geometrisch notwendigen Scherung als Funktion der Migrationsrate einerseits, und der Effizienz der Scherungskompensation durch ruckartiges Korngrenzengleiten andererseits als Funktion der Temperatur. Sobald die Scherung nicht vollständig durch das Korngrenzengleiten kompensiert werden kann, wächst eine Scherspannung bis zu einem kritischen Wert für lokale plastische Verformungen. Die andere Konkurrenz sollte für die Großwinkelkorngrenzen bei hohen Temperaturen auftreten. Die Konkurrenz besteht zwischen der Eintrittsgeschwindigkeit der Atome in eine stark gestörte Korngrenze und der Effizienz des Verlusts der Kristallinität der Atome durch Korngrenzendiffusion. Diese Konkurrenz ist für den Wechsel des Migrationsmechanismus bei Variation der Stärke der treibenden Kraft verantwortlich.

Basierend auf unseren Ergebnissen werden zwei qualitative Mechanismenkarten für Kleinwinkel- bzw. Großwinkelkorngrenzen vorgeschlagen. Diese Vorschläge wurden auch durch verschiedene frühere Beobachtungen der Korngrenzenmigration sowohl in Experimenten als auch in Simulationen verifiziert. Diese früheren Beobachtungen standen oft im Widerspruch zueinander. Sie sind aber kompatibel mit unseren Mechanismenkarten überein.

Nach Kenntnis der Migrationsmechanismen wurden die Mobilitäten für <111>-orientierte Korngrenzen bei hoher Temperatur (0,8Tm) ausgewertet. Hierbei wurde das Verhältnis zwischen der Korngrenzengeschwindigkeit und der Antriebskraft untersucht. Dieses ist nichtlinear und unabhängig vom zugrunde liegenden Mechanismus DISBM oder DIFBM. Es wurde weiter festgestellt, dass das nichtlineare Verhältnis in voller Übereinstimmung mit der Ratentheorie für große Antriebskräfte ist. Mit Hilfe dieser Theorie für die nichtlineare Auswertung wurden die Mobilitäten der Korngrenzen für realistisch geringe Antriebskräfte abgeleitet. Die berechneten Mobilitäten zeigen, dass Großwinkelkorngrenzen viel mobiler als Kleinwinkelkorngrenzen sind, mit einem Mobilitätsmaximum bei etwa 40°. All diese Ergebnisse sind im Einklang mit experimentellen Beobachtungen zu Rekristallisation und Kornwachstum.

Zugleich liefert dieses Auswertungsverfahren ein effektives Volumen, das mit dem zugrunde liegenden Migrationsmechanimus verknüpft ist. Die berechneten Volumen variieren im Bereich von 20 bis zu 61 Atomvolumen. Dieses große Volumen liefert einen zusätzlichen Hinweis, dass die Korngrenzenmigration in der Tat durch DISBM über korrelierte Bewegung von Atomgruppen ermöglicht wird. Es lässt auch vermuten, dass auch für die Migration durch DIFBM sich ganze Atomgruppen vom schrumpfenden Korn lösen und, nach Diffusion in einer rauen Korngrenze, am wachsenden Korn wieder rekonstruieren müssen. Da die effektiven Volumen groß sein können, müssen grundsätzlich alle Mobilitätsauswertungen aus Simulationen angetriebener Korngrenzen durch die nichtlineare Ratentheorie erfolgen, mit zumindest zwei unterschiedlich großen Antriebskräften.

Des Weiteren ist die 38.21° Σ7 Korngrenze im Detail für den Vergleich mit der Literatur untersucht worden. Im Vergleich zu anderen molekulardynamik-simulierten Ergebnissen für diese Korngrenze, hat die hier simulierte Mobilität bei weitem den kleinsten Wert. Dieser Wert liegt in der Nähe der in der Literatur publizierten maximalen experimentellen Ergebnisse. Für diese Korngrenze wurde eine Aktivierungsenergie von 0,74 eV ermittelt. Diese Größe stellt (mit Abstand) den größten Wert dar, der jemals in MD-Simulationen ermittelt worden ist. Dieser Wert liegt recht nahe an dem minimalen experimentellen Wert von 0,7 eV für einen Aluminium Bikristall hoher Reinheit.

Insgesamt hat unser neuer Ansatz der COD-DF-Anwendung gezeigt, dass er Korngrenzenmigration in physikalisch sinnvoller Weise beschreibt. Die Simulationen bieten einen genauen Einblick in die Mechanismen der Korngrenzenmigration. Es zeigt auch das Potential, experimentell vergleichbare Werte für die Mobilität sowie die Aktivierungsparameter vorherzusagen.

Reference

[1]   Rittner JD, Seidman DN. <110> symmetric tilt grain-boundary structures in fcc metals with low stacking-fault energies. Physical Review B 1996;54:6999.

[2]   Gottstein G. Physical Foundations of Materials Science: Springer, 2004.

[3]   Wolf D, Yamakov V, Phillpot SR, Mukherjee A, Gleiter H. Deformation of nanocrystalline materials by molecular-dynamics simulation: relationship to experiments? Acta Materialia 2005;53:1.

[4]   Hasson G, Boos JY, Herbeuval I, Biscondi M, Goux C. Theoretical and experimental determinations of grain boundary structures and energies: Correlation with various experimental results. Surface Science 1972;31:115.

[5]   Keblinski P, Wolf D, Phillpot SR, Gleiter H. Self-diffusion in high-angle fcc metal grain boundaries by molecular dynamics simulation. Philosophical Magazine A 1999;79:2735.

[6]   Mishin Y, Boettinger WJ, Warren JA, McFadden GB. Thermodynamics of grain boundary premelting in alloys. I. Phase-field modeling. Acta Materialia 2009;57:3771.

[7]   Yoon B-K, Choi S-Y, Yamamoto T, Ikuhara Y, Kang S-JL. Grain boundary mobility and grain growth behavior in polycrystals with faceted wet and dry boundaries. Acta Materialia 2009;57:2128.

[8]   Yoon DY, Cho YK. Roughening transition of grain boundaries in metals and oxides. Journal of Materials Science 2005;40:861.

[9]   Olmsted DL, Foiles SM, Holm EA. Grain boundary interface roughening transition and its effect on grain boundary mobility for non-faceting boundaries. Scripta Materialia 2007;57:1161.

[10]   Cahn JW, Mishin Y, Suzuki A. Coupling grain boundary motion to shear deformation. Acta Materialia 2006;54:4953.

[11]   Gottstein G, Shvindlerman LS. Grain Boundary Migration in Metals: Thermodynamics, Kinetics, Applications. Boca Raton, Florida: CRC, 2010 2nd ed.

[12]   Fridman EM, Kopezky CV, Shvindlerman LS. effects of orientation and concentration factors on migration of individual grain boundary in aluminum. Zeitschrift Fur Metallkunde 1975;66:533.

[13]   Winning M, Gottstein G, Shvindlerman LS. Stress induced grain boundary motion. Acta Materialia 2001;49:211.

[14]   Winning M, Gottstein G, Shvindlerman LS. Migration of grain boundaries under the influence of an external shear stress. Materials Science and Engineering a-Structural Materials Properties Microstructure and Processing 2001;317:17.

[15]   Winning M, Gottstein G, Shvindlerman LS. On the mechanisms of grain boundary migration. Acta Materialia 2002;50:353.

[16]   Winning M. Motion of [100] tilt grain boundaries. Acta Materialia 2003;51:6465.

[17]   Winning M, Rollett AD. Transition between low and high angle grain boundaries. Acta Materialia 2005;53:2901.

[18]   Lu YP, Molodov DA, Gottstein G. Recrystallization kinetics and microstructure evolution during annealing of a cold-rolled Fe-Mn-C alloy. Acta Materialia 2011;59:3229.

[19]   Huang Y, Humphreys FJ. Measurements of grain boundary mobility during recrystallization of a single-phase aluminium alloy. Acta Materialia 1999;47:2259.

[20]   Huang Y, Humphreys FJ. Subgrain growth and low angle boundary mobility in aluminium crystals of orientation {110}<001>. Acta Materialia 2000;48:2017.

[21]   Yamakov V, Moldovan D, Rastogi K, Wolf D. Relation between grain growth and grain-boundary diffusion in a pure material by molecular dynamics simulations. Acta Materialia 2006;54:4053.

[22]   Mott NF. slip at grain boundaries and grain growth in metals. Proceedings of the Physical Society of London 1948;60:391.

[23]   Gleiter H. Theory of grain boundary migration rate. Acta Metallurgica 1969;17:853.

[24]   Gleiter H. mechanism of grain boundary migration. Acta Metallurgica 1969;17:565.

[25]   Babcock SE, Balluffi RW. GRAIN-BOUNDARY KINETICS .2. INSITU OBSERVATIONS OF THE ROLE OF GRAIN-BOUNDARY DISLOCATIONS IN HIGH-ANGLE BOUNDARY MIGRATION. Acta Metallurgica 1989;37:2367.

[26]   Jhan RJ, Bristowe PD. A MOLECULAR-DYNAMICS STUDY OF GRAIN-BOUNDARY MIGRATION WITHOUT THE PARTICIPATION OF SECONDARY GRAIN-BOUNDARY DISLOCATIONS. Scripta Metallurgica Et Materialia 1990;24:1313.

[27]   Schoenfelder B, Gottstein G, Shvindlerman LS. Comparative study of grain-boundary migration and grain-boundary self-diffusion of [001] twist-grain boundaries in copper by atomistic simulations. Acta Materialia 2005;53:1597.

[28]   Schoenfelder B, Gottstein G, Shvindlerman LS. Atomistic simulations of grain boundary migration in copper. Metallurgical and Materials Transactions A 2006;37:1757.

[29]   Zhang H, Srolovitz DJ. Simulation and analysis of the migration mechanism of Sigma 5 tilt grain boundaries in an fcc metal. Acta Materialia 2006;54:623.

[30]   Zhang H, Srolovitz DJ, Douglas JF, Warren JA. Characterization of atomic motion governing grain boundary migration. Physical Review B 2006;74:115404.

[31]   Zhang H, Srolovitz DJ, Douglas JF, Warren JA. Atomic motion during the migration of general [001] tilt grain boundaries in Ni. Acta Materialia 2007;55:4527.

[32]   Zhang H, Srolovitz DJ, Douglas JF, Warren JA. Grain boundaries exhibit the dynamics of glass-forming liquids. Proceedings of the National Academy of Sciences of the United States of America 2009;106:7735.

[33]   Yan X, Zhang H. On the atomistic mechanisms of grain boundary migration in [0??] twist boundaries: Molecular dynamics simulations. Computational Materials Science 2010;48:773.

[34]   Shiga M, Shinoda W. Stress-assisted grain boundary sliding and migration at finite temperature: A molecular dynamics study. Physical Review B 2004;70.

[35]   Cahn JW, Taylor JE. A unified approach to motion of grain boundaries, relative tangential translation along grain boundaries, and grain rotation. Acta Materialia 2004;52:4887.

[36]   Caillard D, Mompiou F, Legros M. Grain-boundary shear-migration coupling. II. Geometrical model for general boundaries. Acta Materialia 2009;57:2390.

[37]   Suzuki A, Mishin Y. Atomic mechanisms of grain boundary motion. Materials Science Forum 2005;502:157.

[38]   Mishin Y, Suzuki A, Uberuaga BP, Voter AF. Stick-slip behavior of grain boundaries studied by accelerated molecular dynamics. Physical Review B 2007;75.

[39]   Ivanov VA, Mishin Y. Dynamics of grain boundary motion coupled to shear deformation: An analytical model and its verification by molecular dynamics. Physical Review B 2008;78.

[40]   Zhang H, Du D, Srolovitz DJ. Effects of boundary inclination and boundary type on shear-driven grain boundary migration. Philosophical Magazine 2008;88:243.

[41]   Molodov DA, Ivanov VA, Gottstein G. Low angle tilt boundary migration coupled to shear deformation. Acta Materialia 2007;55:1843.

[42]   Gorkaya T, Molodov DA, Gottstein G. Stress-driven migration of symmetrical <100> tilt grain boundaries in Al bicrystals. Acta Materialia 2009;57:5396.

[43]   Sheikh-Ali AD. Coupling of grain boundary sliding and migration within the range of boundary specialness. Acta Materialia 2010;58:6249.

[44]   Gianola DS, Van Petegem S, Legros M, Brandstetter S, Van Swygenhoven H, Hemker KJ. Stress-assisted discontinuous grain growth and its effect on the deformation behavior of nanocrystalline aluminum thin films. Acta Materialia 2006;54:2253.

[45]   Legros M, Gianola DS, Hemker KJ. In situ TEM observations of fast grain-boundary motion in stressed nanocrystalline aluminum films. Acta Materialia 2008;56:3380.

[46]   Mompiou F, Caillard D, Legros M. Grain boundary shear-migration coupling-I. In situ TEM straining experiments in Al polycrystals. Acta Materialia 2009;57:2198.

[47]   Rupert TJ, Gianola DS, Gan Y, Hemker KJ. Experimental Observations of Stress-Driven Grain Boundary Migration. Science 2009;326:1686.

[48]   Sharon JA, Su PC, Prinz FB, Hemker KJ. Stress-driven grain growth in nanocrystalline Pt thin films. Scripta Materialia 2011;64:25.

[49]   Bernstein N. The influence of geometry on grain boundary motion and rotation. Acta Materialia 2008;56:1106.

[50]   Pond RC, Smith DA. ABSORPTION OF DISLOCATIONS BY GRAIN-BOUNDARIES. Philosophical Magazine 1977;36:353.

[51]   Babcock SE, Balluffi RW. GRAIN-BOUNDARY KINETICS .1. INSITU OBSERVATIONS OF COUPLED GRAIN-BOUNDARY DISLOCATION-MOTION, CRYSTAL TRANSLATION AND BOUNDARY DISPLACEMENT. Acta Metallurgica 1989;37:2357.

[52]   Zhang H, Mendelev MI, Srolovitz DJ. Computer simulation of the elastically driven migration of a flat grain boundary. Acta Materialia 2004;52:2569.

[53]   Mishin Y, Asta M, Li J. Atomistic modeling of interfaces and their impact on microstructure and properties. Acta Materialia 2010;58:1117.

[54]   Schoenfelder B, Wolf D, Phillpot SR, Furtkamp M. Molecular-Dynamics Method for the Simulation of Grain-Boundary Migration. Interface Science 1997;5:245.

[55]   Upmanyu M, Smith RW, Srolovitz DJ. Atomistic simulation of curvature driven grain boundary migration. Interface Science 1998;6:41.

[56]   Upmanyu M, Srolovitz DJ, Shvindlerman LS, Gottstein G. Misorientation dependence of intrinsic grain boundary mobility: simulation and experiment. Acta Materialia 1999;47:3901.

[57]   Upmanyu M, Srolovitz DJ, Shvindlerman LS, Gottstein G. Molecular dynamics simulation of triple junction migration. Acta Materialia 2002;50:1405.

[58]   Zhang H. Atomistic simulation of sliding of [10(1)over-bar0] tilt grain boundaries in Mg. Journal of Materials Research 2009;24:3446.

[59]   Zhang H, Mendelev MI, Srolovitz DJ. Mobility of [Sigma]5 tilt grain boundaries: Inclination dependence. Scripta Materialia 2005;52:1193.

[60]   Zhang H, Upmanyu M, Srolovitz DJ. Curvature driven grain boundary migration in aluminum: molecular dynamics simulations. Acta Materialia 2005;53:79.

[61]   Zhou L, Zhang H, Srolovitz DJ. A size effect in grain boundary migration: A molecular dynamics study of bicrystal thin films. Acta Materialia 2005;53:5273.

[62]   Godiksen RB, Trautt ZT, Upmanyu M, Schioz J, Juul Jensen D, Schmidt S. Simulations of boundary migration during recrystallization using molecular dynamics. Acta Materialia 2007;55:6383.

[63]   Godiksen RB, Trautt ZT, Upmanyu M, Schmidt S, Jensen DJ. simulation of recrystallization using Molecular Dynamics; effects of the interatomic potential. Materials Science Forum 2007.

[64]   Godiksen RB, Trautt ZT, Upmanyu M, Schmidt S, Juul Jensen D. Towards atomic level simulations of recrystallisation - setting up suitable geometry. Materials Science and Technology 2005;21:1373.

[65]   Godiksen RBN, Schmidt S, Juul Jensen D. Molecular dynamics simulations of grain boundary migration during recrystallization employing tilt and twist dislocation boundaries to provide the driving pressure. Modelling and Simulation in Materials Science and Engineering 2008;16:065002.

[66]   Foiles SM, Hoyt JJ. Computation of grain boundary stiffness and mobility from boundary fluctuations. Acta Materialia 2006;54:3351.

[67]   Trautt ZT, Upmanyu M, Karma A. Interface Mobility from Interface Random Walk. Science 2006;314:632.

[68]   Lobkovsky AE, Karma A, Mendelev MI, Haataja M, Srojovitz DJ. Grain shape, grain boundary mobility and the Herring relation. Acta Materialia 2004;52:285.

[69]   Janssens KGF, Olmsted D, Holm EA, Foiles SM, Plimpton SJ, Derlet PM. Computing the mobility of grain boundaries. Nature Materials 2006;5:124.

[70]   Olmsted DL, Holm EA, Foiles SM. Survey of computed grain boundary properties in face-centered cubic metals--II: Grain boundary mobility. Acta Materialia 2009;57:3704.

[71]   Hoyt JJ, Trautt ZT, Upmanyu M. Fluctuations in molecular dynamics simulations. Mathematics and Computers in Simulation 2010;80:1382.

[72]   Molodov DA, Czubayko U, Gottstein G, Shvindlerman LS. MOBILITY OF 111 TILT GRAIN-BOUNDARIES IN THE VICINITY OF THE SPECIAL MISORIENTATION SIGMA=7 IN BICRYSTALS OF PURE ALUMINUM. Scripta Metallurgica Et Materialia 1995;32:529.

[73]   Molodov DA, Czubayko U, Gottstein G, Shvindlerman LS. On the effect of purity and orientation on grain boundary motion. Acta Materialia 1998;46:553.

[74]   Molodov DA, Czubayko U, Gottstein G, Shvindlerman LS, Straumal B, Gust W. Acceleration of grain boundary motion in Al by small additions of Ga. Philosophical Magazine Letters 1995;72:361

[75]   Molodov DA, Gorkaya T, Gottstein G. Mechanically driven migration of < 100 > tilt grain boundaries in Al-bicrystals. In: Kang SJL, Huh MY, Hwang NM, Homma H, Ushioda K, Ikuhara Y, editors. 3rd International Conference on Recrystallization and Grain Growth, ReX and GG III. Jeju Isl, SOUTH KOREA, 2007. p.927.

[76]   Molodov DA, Gottstein G, Heringhaus F, Shvindlerman LS. Motion of planar grain boundaries in bismuthbicrystals driven by a magnetic field. Scripta Materialia 1997;37:1207.

[77]   Molodov DA, Gottstein G, Heringhaus F, Shvindlerman LS. True absolute grain boundary mobility: motion of specific planar boundaries inBi-bicrystals under magnetic driving forces. Acta Materialia 1998;46:5627.

[78]   Kopetsky CV, Shvindlerman LS, Sursaeva VG. effect of athermal motion of grain boundaries. Scripta Metallurgica 1978;12:953.

[79]   Maksimova EL, Shvindlerman LS, Straumal BB. TRANSFORMATION OF SIGMA-17 SPECIAL TILT BOUNDARIES TO GENERAL BOUNDARIES IN TIN. Acta Metallurgica 1988;36:1573.

[80]   Badirujjaman S, Li X-W, Winning M. Motion of [100]-tilt grain boundaries under cyclic stresses. Materials Science and Engineering: A 2007;448:242.

[81]   Winning M. Feature article: Influencing grain boundary properties by the application of mechanical stress fields. Physica Status Solidi a-Applied Research 2004;201:2867.

[82]   Winning M. Stress-induced migration of tilt and twist grain boundaries. International Journal of Materials Research 2004;95:233.

[83]   Winning M. In-situ observations of coupled grain boundary motion. Philosophical Magazine 2007;87:5017.

[84]   Winning M. Strain-induced migration of tilt grain boundaries. Scripta Materialia 2008;58:85.

[85]   Winning M, Rollett AD, Gottstein G, Srolovitz DJ, Lim A, Shvindlerman LS. Mobility of low-angle grain boundaries in pure metals. Philosophical Magazine 2010;90:3107

[86]   Fukutomi H, Horiuchi R. STRESS-INDUCED MIGRATION OF SYMMETRIC TILT BOUNDARIES IN ALUMINUM. Transactions of the Japan Institute of Metals 1981;22:633.

[87]   Gorkaya T, Molodov KD, Molodov DA, Gottstein G. Concurrent grain boundary motion and grain rotation under an applied stress. Acta Materialia 2011;59:5674.

[88]   Günster C, Molodov DA, Gottstein G. Magnetically driven migration of specific planar grain boundaries in Zn. Scripta Materialia 2010.

[89]   Andersen HC. Molecular dynamics simulations at constant pressure and/or temperature. The Journal of Chemical Physics 1980;72:2384.

[90]   Cleri F, Rosato V. Tight-binding potentials for transition metals and alloys. Physical Review B 1993;48:22.

[91]   Morris JR, Song XY. The anisotropic free energy of the Lennard-Jones crystal-melt interface. Journal of Chemical Physics 2003;119:3920.

[92]   Li J. AtomEye: an efficient atomistic configuration viewer. Modelling and Simulation in Materials Science and Engineering 2003;11:173.

[93]   Balluffi RW, Cahn JW. MECHANISM FOR DIFFUSION INDUCED GRAIN-BOUNDARY MIGRATION. Acta Metallurgica 1981;29:493.

[94]   Smith DA, King AH. ON THE MECHANISM OF DIFFUSION-INDUCED BOUNDARY MIGRATION. Philosophical Magazine a-Physics of Condensed Matter Structure Defects and Mechanical Properties 1981;44:333.

[95]   Yamamoto Y, Kajihara M. Quantitative analysis of observations on diffusion induced grain boundary migration for random boundaries in the Cu(Zn) system using a driving force model. Acta Materialia 1999;47:1195.

[96]   Yamamoto Y, Moriyama M, Kajihara M, Mori T. Kinetics of diffusion induced grain boundary migration of [100] twist boundaries in the Cu(Zn) system. Acta Materialia 1999;47:1757.

[97]   Goukon N, Ikeda T, Kajihara M. Characteristic features of diffusion induced grain boundary migration for Sigma 9 [110] asymmetric tilt boundaries in the Cu(Zn) system. Acta Materialia 2000;48:1551.

[98]   Meyers MA, Mishra A, Benson DJ. Mechanical properties of nanocrystalline materials. Progress in Materials Science 2006;51:427.

[99]   Ivanov VA, Molodov DA, Shvindlerman LS, Gottstein G. Impact of boundary orientation on the motion of curved grain boundaries in aluminum bicrystals. In: Bacroix B, Driver JH, LeGall R, Maurice C, Penelle R, Regle H, Tabourot L, editors. Recrystallization and Grain Growth, Pts 1 and 2, vol. 467-470. Zurich-Uetikon: Trans Tech Publications Ltd, 2004. p.751.

[100]   Schoenfelder B, Keblinski P, Wolf D, Phillpot SR. On the Relationship between Grain-Boundary Migration and Grain-Boundary Diffusion by Molecular-Dynamics Simulation. Materials Science Forum 1999;294-296:9.

[101]   Bachurin DV, Weygand D, Gumbsch P. Dislocation-grain boundary interaction in <111> textured thin metal films. Acta Materialia 2010;58:5232.

[102]   Ye F, Lu K. Crystallization kinetics of amorphous solids under pressure. Physical Review B 1999;60:7018.

Curriculum Vitae

Personal data

Name: Jian Zhou

Date and place of birth: 16.03.1981, Wujiang China

Marital status: Single

Nationality: Chinese

Education

1999 - 2003   Bachelor of science in Biomedical Engineering,
                               Southeast University, China.

2003 - 2005   Master of science (M. Sc.) in Biomedical Engineering,
                               Southeast University, China.

10/2005 - 11/2007   M. Sc. in Advanced Materials, Ulm University, Germany

03/2008 - 02/2012   A doctoral candidate in the Institut für Metallkunde und
                               Metallphysik, RWTH Aachen University, Germany

Publications

1. Zhou[*] J, Mohles V. *Mobility evaluation of <110> twist grain boundary motion from molecular dynamics simulation*. **Steel Research International** 2011;82:114.

2. Zhou[*] J, Mohles V. *Towards realistic molecular dynamics simulations of grain boundary mobility*. **Acta Materialia** 2011;59:5997.

3. Zhou[*] J, Mohles V. *A generalized migration mechanism of symmetric tilt grain boundaries in molecular dynamics simulations.* Submitted to **Modelling and Simulation in Materials Science and Engineering** in Feb. 2012.